

Contents lists available at ScienceDirect

# Transportation Research Part C

journal homepage: www.elsevier.com/locate/trc



# Dynamic joint decision of matching parameters and relocation strategies in ride-sourcing systems interacting with traffic congestion

Jun Zhang <sup>a,b</sup>, Lu Hu <sup>a,b,\*</sup>, Yan Li <sup>c</sup>, Weiyao Xu <sup>a,b</sup>, Yangsheng Jiang <sup>a,b</sup>

- <sup>a</sup> School of Transportation and Logistics, Southwest Jiaotong University, Chengdu, 610031, China
- b National Engineering Laboratory of Integrated Transportation Big Data Application Technology, Chengdu, 610031, China
- <sup>c</sup> Department of Industrial Systems Engineering and Management, National University of Singapore, Singapore

#### ARTICLE INFO

# Keywords: Ride-sourcing system Relocation strategy Online matching Congestion effects Simulation-based optimization Bayesian optimization

#### ABSTRACT

As the ride-sourcing market expands, ride-sourcing fleets have increased urban traffic congestion, and in turn, road congestion is affecting ride-sourcing operations. It is crucial to incorporate this interaction mechanism into the operational decision of ride-sourcing systems. This mechanism can be described in detail by simulation models. Applying simulation-based optimization methods to the real-time operation of ride-sourcing systems is challenging due to the limitations of simulation efficiency. To tackle this issue, this study first proposes a modular simulation model combining time-driven and event-driven mechanisms. The simulation model comprises two layers: the traffic flow module at the bottom, defined by trip-based and multiregion macroscopic fundamental diagrams and cell transmission models, and the ride-sourcing operation module at the top, which considers the interaction between the traffic congestion and ride-sourcing operation and models the random behavior of passengers and drivers. We verify the efficiency and accuracy of the simulation model. The simulation model is utilized as an evaluator of the objective functions and performance measures. Then, we integrate the Bayesian optimization, parallel sampling, and rolling horizon approaches to develop an efficient and effective simulation-based optimization framework for the dynamic joint decisionmaking of matching radius, matching intervals, and threshold relocation strategies. Six groups of experiments for the traffic scenario in Berlin reveal some interesting findings. (1) The matching rate first increases and then decreases with the matching radius (a concave function), while the closest study does not think so. (2) As the fleet size grows, passenger waiting time reaches its minimum and then rises because of the increased endogenous congestion generated by ridesourcing fleets. (3) The optimal operation strategy considering endogenous congestion not only leads to an increase in the system revenue and efficiency but also leads to congestion relief, even though the latter was not our initial objective. This benefit is the most pronounced when the fleet size and background traffic are moderate.

#### 1. Introduction

Ride-sourcing systems have revolutionized the transportation industry by providing commuters with a reliable and convenient mode of transportation. Popular service platforms like Uber, Lyft, and DiDi have emerged as viable alternatives to traditional taxi

<sup>\*</sup> Corresponding author at: School of Transportation and Logistics, Southwest Jiaotong University, Chengdu, 610031, China. E-mail address: hulu@swjtu.edu.cn (L. Hu).

services. These platforms collect and analyze real-time data on drivers and passengers and use centralized matching algorithms to assign drivers to passengers before they meet. Effectively leveraging this data to optimize fleet operations can increase revenues for platforms and drivers while reducing waiting times for passengers.

Matching and order dispatching is one of the most fundamental operational problems for ride-sourcing platforms, which affect the overall performance and efficiency of ride-sourcing systems significantly (Wang and Yang, 2019). Bipartite graph matching between idle drivers and passengers is a widely adopted matching strategy (Xu et al., 2018), which contains two key parameters that affect the efficiency of the system, the matching radius and the matching time interval. Deliberately controlling the matching time interval can regulate the buffer size of potential matches and enhance operational efficiency (Qin et al., 2021b). And adaptively adjusting the matching radius, throughput loss can be avoided (Xu et al., 2020b). The optimal choice of these two parameters is very dependent on the real-time supply and demand states (Yang et al., 2020), and the relocation strategy is an important tool for balancing supply and demand in the ride-sourcing market. Hence, optimizing these two parameters jointly with the relocation strategy is necessary. Most approaches used to solve the matching parameter or relocation strategy problem are either analytical models or reinforcement learning methods (Ke et al., 2022; Zhou et al., 2020). However, dynamically and jointly optimizing the matching radius, matching time interval, and relocation strategy is a significant challenge due to the intractability of these methods in relaxing strict assumptions or training models. As far as we know, the current literature does not provide a solution to this problem although some research integrates the pregiven relocation strategy (or matching strategy) into the matching (or relocation) optimization problem (Alonso-Mora et al., 2017; Bischoff and Maciejewski, 2020). Addressing this joint optimization problem necessitates the utilization of a comprehensive system dynamics model. This model should effectively capture the intricate interactions among the matching radius. matching time interval, and relocation strategy, instead of integrating these factors into a singular strategy.

Imbalances in supply and demand lead drivers to cruise on the road until they match the next passenger, resulting in extended waiting times for passengers and reduced earnings for drivers. Drivers can even spend up to 50% of their time searching for passengers (Xu et al., 2020a). To address this issue, researchers have developed various relocation strategies to improve ride-sourcing system performance (Xu et al., 2020a; Zhou et al., 2020). The primary objective of these studies is to encourage drivers in low-demand areas to move to high-demand areas as much as possible, disregarding the negative impacts of endogenous congestion generated by ride-sourcing fleets. When the dynamics of congestion are omitted in ride-sourcing studies, and the focus is solely on matching strategies or vehicle relocation strategies in static environments, the conclusions drawn may differ and lead to potentially unrealistic performance measures (Beojone and Geroliminis, 2021). To the best of our knowledge, no studies have considered both endogenous congestion (generated by ride-sourcing fleet) and exogenous congestion (generated by background traffic) in the operational decision-making of ride-sourcing systems. Therefore, our objective is no longer solely to optimize the operational efficiency of the ride-sourcing system in a static traffic environment but to make a trade-off between satisfying demand and mitigating the adverse effects of dynamic traffic congestion.

Simulation-based optimization may offer a more tractable approach to addressing the aforementioned issues than analytical model-based optimization or reinforcement learning methods. On one hand, analytical models face difficulties in accurately capturing interactions among decision variables due to their strict assumptions. On the other hand, reinforcement learning models encounter several challenges when addressing this issue. These challenges include handling continuous decision variables, managing large-scale state spaces caused by endogenous congestion, training an appropriate reward function that aligns with the desired objectives, and facilitating collaborative decision-making across multiple regions. Additionally, the real-time data collected during ride-sourcing operations is well-suited for constructing simulation models or even digital twin models (Liu et al., 2021). A few pieces of literature on simulation-based optimization for autonomous mobility-on-demand systems focus on the planning stage instead of the operational stage. For example, Bischoff et al. (2018) optimize the service area for ride-sourcing operators. Dandl et al. (2021) optimize public transportation budgets and fleet size limits. Because the computation of the simulation model is generally time-consuming, it is challenging to make operational decisions within tightly computed budgets. This study attempts to address the problem of the computational efficiency of simulation models and develop a practical simulation-based optimization framework to optimize matching parameters and relocation strategies.

Hence, the goal of this study is twofold: First, we aim to develop a traffic simulation model that is both computationally efficient and accurate. To achieve this, we propose a macroscopic modeling approach that incorporates both endogenous and exogenous congestion in ride-sourcing systems. Our approach is based on the utilization of the Macroscopic Fundamental Diagram (MFD) and Cell Transmission Model (CTM) frameworks. Second, we aim to establish an efficient and effective simulation-based optimization framework. To accomplish this, we employ an improved Bayesian optimization (BO) technique. This involves utilizing a multi-objective acquisition function, implementing input wrapping techniques, and enabling parallel sampling. The optimization is carried out on a rolling horizon, allowing for dynamic and adaptive decision-making.

The main contributions of this paper are as follows:

(1) We develop a trip-based and multi-region MFD traffic dynamics simulation model to strike a balance between accuracy and efficiency by appropriately capturing the interaction between traffic congestion and ride-sourcing system operation. The model utilizes the CTM to clearly depict the propagation of congestion across region boundaries. We customize a hybrid of time-driven and event-driven mechanisms to accelerate the simulation process. Notice that our model extends the trip-based MFD traffic dynamics model of Beojone and Geroliminis (2021) by considering the multi-region MFD, congestion prorogation, and hybrid-driven mechanism. These extensions significantly improve the efficiency and accuracy of the proposed simulation model, making simulation-based optimization available under the real-time operational stage of the ride-sourcing system. We validate the accuracy of this simulation model by the real-world data.

- (2) We introduce a threshold-based relocation strategy with compensation to incentivize drivers to participate in relocation tasks. Additionally, drivers possibly reject relocation tasks and choose random cruising or staying, which is closer to real-world scenarios.
- (3) We also consider the interaction among the optimal matching radius, matching time interval, and relocation strategy. To dynamically achieve joint optimization of the matching and relocation strategies of multiple sub-regions, a simulation-based optimization framework has been developed. This framework employs the improved BO with a multi-objective acquisition function to solve the black-box stochastic optimization problem. Additionally, parallel sampling and rolling horizon approaches are employed to effectively reduce the optimization computational time.
- (4) By conducting six groups of numerical experiments for the traffic scenario in Berlin, we obtain some insights that differ from the closest study. For instance, Yang et al. (2020) showed that the matching rate first increases with the matching radius, but becomes independent of the matching radius once it exceeds a certain threshold (around 700 m). Conversely, our results indicate that the matching rate first increases and subsequently decreases with the matching radius (a concave function), and we observed that the matching rate continues to be affected by the matching radius, even at a great value (4400 m).

The remainder of this paper is organized as follows: Section 2 provide a comprehensive review of the relevant literature on the topic. Section 3 elaborates the problem and the basic assumptions. Section 4 presents the proposed simulation models, including the traffic flow model, ride-sourcing system operation model, as well as their connections. Section 5 introduces a simulation-based optimization framework for determining the optimal matching and relocation strategy parameters for each sub-region. Section 6 presents several computational experiments, including simulation accuracy verification, critical parameter sensitivity analysis, performance test of the simulation-based optimization framework, comparison of different optimization algorithms, and comparison of best solutions with and without endogenous congestion. Finally, Section 7 concludes this work with key findings and future research directions.

#### 2. Literature review

Our research has focused on the intersection of five critical issues: (1) the matching problem, (2) the relocation problem, (3) the joint operational strategy, (4) the interaction between traffic congestion and ride-sourcing systems, and (5) the modeling and optimization method. By synthesizing knowledge from these fields, we aim to provide valuable insights into operational strategy in ride-sourcing systems.

#### 2.1. Matching problem

The online matching problem was initially studied by Yang et al. (2010) as a bilateral taxi-passengers search problem. In ridesourcing systems, the dispatch model has been generally adopted owing to its advantage of minimizing the overall pick-up cost of all drivers. Considering the structural characteristics of the bipartite graph, it is commonly formulated as an integer optimization or combinatorial optimization problem. For example, Vazifeh et al. (2018) proposed a vehicle-sharing network to assign passengers to drivers while minimizing the fleet size. Bertsimas et al. (2019) developed a mixed-integer programming model to maximize operational profits in taxi dispatching. Billhardt et al. (2019) introduced an auction algorithm to reassign the taxi-passenger pairs with driver subsidies. Zhao et al. (2019) considered driver and passenger preferences to obtain a stable match between them. Heuristic algorithms are commonly employed to overcome the curse of dimensionality in this problem (Wang and Yang, 2019).

In contrast to the aforementioned studies, some research explores the execution time of the matching strategy (matching time interval) instead of instant matching, as well as the limitations on the matching distance (matching radius). Several studies employed specific system dynamics models to conduct their analyses. Ke et al. (2020) developed an aggregate traffic flow model that incorporates the effects of traffic congestion. They investigated the synergies of passenger requests and matching time interval on the opportunity cost of time for passengers of private cars and ride-sourcing and determine their combinations resulting in a win-win situation. Xu et al. (2020b) constructed a two-end queuing model that explicitly incorporates the influence of a finite matching radius, which proved that adaptive matching radius adjustments could completely avoid backward bending of the supply curve. Additionally, some studies have focused on developing efficient algorithms to adjust these two variables dynamically. Aouad and Saritaç (2020) formulated the dynamic matching problem as a Markov decision process and designed a 3-approximation algorithm for minimizing cost in matching problems with uniform abandonment rate. Feng et al. (2022) modeled a ride-sourcing system with block matching via a queue model to decide the proper block size.

## 2.2. Relocation problem

Besides developing an effective matching algorithm, implementing a relocation strategy is crucial for addressing the supply-demand imbalance. The driver relocation or recommendation problem originates from the traditional route-finding problem of taxi drivers. Researchers have suggested various solutions for this problem, which can be classified into two categories: hotspot recommendation and route recommendation. Hotspots refer to areas where high traveling demands and low taxi service supply exist. Ge et al. (2010) developed a recommendation system that provides taxi drivers with information regarding potential pick-up points and parking locations. Powell et al. (2011) proposed spatio-temporal profitability maps to recommend the next profitable location for idle drivers. Similarly, Hwang et al. (2015) proposed a taxi recommender system to determine the next cruising location

by considering the travel distance, waiting time, and expected fare. On the other hand, route recommendation provides a more fine-grained approach. Liu et al. (2015) proposed a non-myopic adaptive route algorithm that considers the collective travel time minimization of all vehicles under uncertain and dynamic congestion conditions. Lai et al. (2019) investigated the attractiveness between taxis and passengers, and the competition among taxis according to Coulomb's law, from which more accurate and effective route recommendations are derived. Within recent years, the Markov Decision Process (MDP) and reinforcement learning (RL) have been brought into the interest of scholars to address such problems (Rong et al., 2016; Zhou et al., 2020; Yu et al., 2019).

#### 2.3. Joint operational strategy

However, the challenge of designing an effective repositioning strategy, while simultaneously adapting the matching parameters (matching time interval and matching radius), to enhance the efficiency of ride-sourcing systems, remains unresolved. In contrast to some predefined joint strategies (Tang et al., 2019; Duan et al., 2020; Guo et al., 2021), effectively determining the optimal combination of matching radius, matching time interval, and relocation strategy requires a more comprehensive system dynamics model capable of capturing their intricate interactions. Gueriau and Dusparic (2018) proposed a decentralized reinforcement learning approach for the joint decision-making of vehicle relocation and ride request assignment in shared mobility-on-demand systems. However, they did not touch on the issue of matching time interval and radius. Tang et al. (2019) employed reinforcement learning to tackle both the matching and relocation problems, but only relocation actions are decided. Regarding the matching problem, the value network is used to solve the pregiven bipartite graph matching problem. Holler et al. (2019) also presented a deep reinforcement learning approach for relocation and matching problems. In their study, the decision for the matching action is made when a driver is within the matching radius, while the relocation action is determined when the driver is outside the matching radius. However, their approach does not involve decisions of matching radius. Hence, to the best of our knowledge, the existing literature lacks a solution for simultaneously optimizing relocation strategies and matching parameters.

#### 2.4. Interaction between traffic congestion and ride-sourcing systems

By means of real data and simulation analyses, a series of studies have confirmed that the growth of the ride-sourcing market exerts a significant influence on the dynamics of urban traffic congestion (Erhardt et al., 2019; Diao et al., 2021), and in turn, the dynamic congestion feeds back into ride-sourcing operations. However, the majority of existing literature on matching or relocation strategies overlooks this interaction effect, resulting in irrational system performance and misleading conclusions (Beojone and Geroliminis, 2021). Integrating both endogenous congestion (generated by ride-sourcing fleets) and exogenous congestion (generated by background traffic) simultaneously into operational decision-making poses a significant challenge. It requires accurate and efficient traffic flow models as well as optimization algorithms. To the best of our knowledge, no studies have successfully addressed this problem, whether through analytical modeling or reinforcement learning approaches.

#### 2.5. Modeling and optimization method

The existing analytical modeling approaches provide effective properties for matching radius and matching time interval (Yang et al., 2020); Xu et al., 2020b; Ke et al., 2020). However, analytical methods may not give good solutions for real-time decision-making in real-world scenarios due to their reliance on strict assumptions. In contrast, reinforcement learning is well-suited for dynamic ride-sourcing system environments that support real-time decisions. Nevertheless, the quality of training data and the complexity of designing states, actions, and rewards present significant challenges in model training. In the literature concerning reinforcement learning for ride-sourcing systems, the state function dictates the agent's actions, but almost all these studies employ tabular state functions without considering endogenous and exogenous congestion information (Qin et al., 2021b; Ke et al., 2022; Tang et al., 2019; Holler et al., 2019). Additionally, the existing reinforcement learning literature typically assumes the driver's full compliance with repositioning instructions (Qin et al., 2022), which may lead to unrealistic performance evaluation.

While simulation-based optimization approaches provide scalable solutions, including but not limited to endogenous and exogenous congestion information, the computational time required by most microscopic or mesoscopic traffic simulation software (e.g. SUMO or MATSim) is expensive. Apart from the complex microscopic computations, the high computational cost of these simulation software arises from their time-driven mechanism, wherein the states of all components are updated at a predefined frequency. This frequency must be large enough to guarantee the accuracy of the simulation. These limitations render black-box optimization approaches (e.g. Bayesian optimization) based on the time-driven microscopic simulation models inapplicable for dynamic operational decision-making of ride-sourcing systems. This is because they cannot make effective decisions within a tight time budget (e.g. 5 or 10 min). Fortunately, recent research has enhanced the simulation efficiency with an event-driven macroscopic traffic simulation approach. For example, Beojone and Geroliminis (2021) proposed a trip-based Macroscopic Fundamental Diagram (MFD) traffic dynamics model, which characterizes the entire road network with an MFD, and used an event-driven simulation mechanism. However, the simulation efficiency is limited when there are numerous events, especially with a large number of trips. Moreover, using a single MFD may lead to inaccuracy as it does not account for congestion propagation (queue spillback) among multiple sub-regions. Therefore, there is an urgent need for a traffic simulation model with high accuracy and efficiency to facilitate real-time operational decision-making in ride-sourcing system operations.

As summarized in Table 1, the difference or innovation between this paper and others reflects on major attributes. In summary, the existing literature lacks concentration on the joint optimization of matching radius, matching time interval, and relocation

Table 1
Differences between the main relevant literature and this study

Authors	Method type	The optimization pr	Consideration of		
		Matching radius	Matching time interval	Relocation strategy	endogenous congestion
Xu et al. (2020b)	AM				
Ke et al. (2022)	RL	·	$\sqrt{}$		
Qin et al. (2021a)	RL		ý		
Yang et al. (2020)	AM		ý		
Aouad and Saritaç (2020)	MDP	•	ý		
Zhou et al. (2020)	MDP		·	$\sqrt{}$	
Holler et al. (2019)	RL			ý	
Duan et al. (2020) <sup>a</sup>	AM			ý	
Guo et al. (2021) <sup>a</sup>	AM			ý	
Tang et al. (2019) <sup>a</sup>	RL			·	
This study	SBO		$\sqrt{}$	·	$\sqrt{}$

AM: Analytical model; RL: Reinforcement learning; MDP: Markov decision process; SBO: Simulation-based optimization.

strategy in the ride-sourcing system. Furthermore, there is still a notable gap in integrating endogenous congestion into dynamic operational decision-making. This study aims to bridge these gaps by developing a simulation-based optimization framework to solve the dynamic operational problem in ride-sourcing systems. Our simulation model takes endogenous and exogenous traffic congestion, random order cancellations, idle driver random cruise, and possible neglect of relocation into consideration to improve the effectiveness of the operation strategy. This study employs a Bayesian optimization framework with a rolling horizon approach to optimize the matching and relocation strategy parameters in each operation sub-region.

#### 3. Problem statement

This study aims to address the operational strategy problem (the joint matching and relocation strategies) in a ride-sourcing system that excludes ride-sharing services among multiple passengers. The matching strategy involves determining the optimal matching radius and matching time interval for all operational sub-regions, while the relocation strategy involves planning the cruising destination for idle drivers to achieve supply-demand equilibrium. If a driver who accepts a relocation task remains unmatched by a passenger for an extended period, the ride-sourcing platform compensates the driver with a predetermined amount.

The matching radius and time interval have a significant impact on the operational performance and passenger experience of a ride-sourcing system. The matching radius determines the maximum distance between passengers and idle drivers for a successful match. As the matching radius expands, the probability of passengers being matched with drivers increases, but it also leads to longer pick-up distances. The matching time interval refers to the duration within which the system searches for available drivers and unmatched passengers. As the matching interval time increases, the probability of passengers being matched with a closer driver increases, but it also leads to longer passenger waiting time and potential order cancellations. Fig. 1 illustrates the impact of these parameters on the system. In the first scenario, the same matching radius is applied to all operational sub-regions, and passengers P1 will continue to wait unless the matching radius R of the sub-region is increased (second scenario) or the matching time interval  $\Delta t$  is extended (third scenario). In complex real-world situations, the optimal strategy depends on the supply-demand status, including the arrival rates of drivers and passengers and the number of drivers and passengers in the matching pool.

The relocation strategy plays a critical role in maintaining the supply-demand balance in a ride-sourcing system. The effectiveness of this strategy relies on the matching radius and matching time interval selected. For instance, adjusting the matching time interval in the scenario presented in Fig. 2 will result in varying supply and demand conditions, and thus it is necessary to adapt the optimal relocation strategy accordingly. As shown in Fig. 3, the matching radius change significantly impacts the optimal relocation strategy. Expanding the matching radius (R1<R2) in a sub-region reduces the number of available drivers for relocation since they have already been matched with passengers. Therefore, it is essential to consider the interdependence between the matching radius, matching time interval, and relocation strategy when formulating a comprehensive operational strategy for a ride-sourcing system.

Furthermore, when considering traffic congestion, idle drivers must be relocated cautiously to sub-regions with high demand yet severe congestion to prevent any adverse effects on operational efficiency. This is because excessive relocation may further worsen the traffic congestion in these sub-regions and lower the vehicle circulation of ride-sourcing systems. In other words, the operation of ride-sourcing systems is closely intertwined with traffic congestion. In this paper, we first develop a simulation model to uncover this interaction. We then propose a simulation-based optimization framework for jointly determining the matching radius, matching time interval, and relocation strategies

There are some assumptions made for the simulation model.

- (1) Once the passenger-driver matching has been completed, neither of them will cancel the order.
- (2) If a passenger remains unmatched with a driver for an extended period after joining the ride-sourcing system, the passenger will cancel the order.
- (3) Upon receiving a relocation task, the driver has a certain probability of acceptance.
- (4) Drivers who have not accepted a relocation task have a certain probability of cruising to a high-demand sub-region/ staying/ cruising nearby within the current sub-region.

<sup>&</sup>lt;sup>a</sup> Predefined joint strategy for matching and relocation problems.

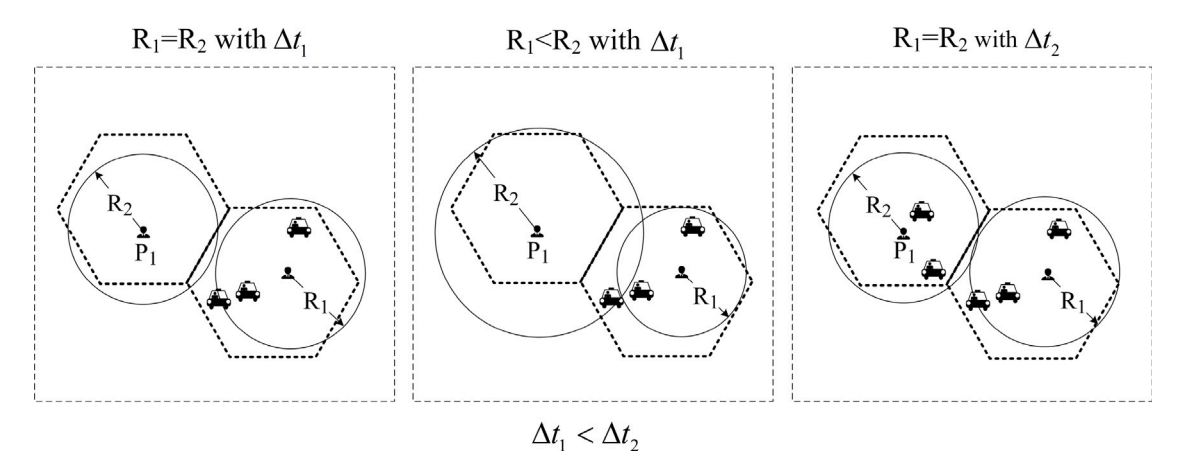


Fig. 1. Joint impact of matching radius and matching time interval.

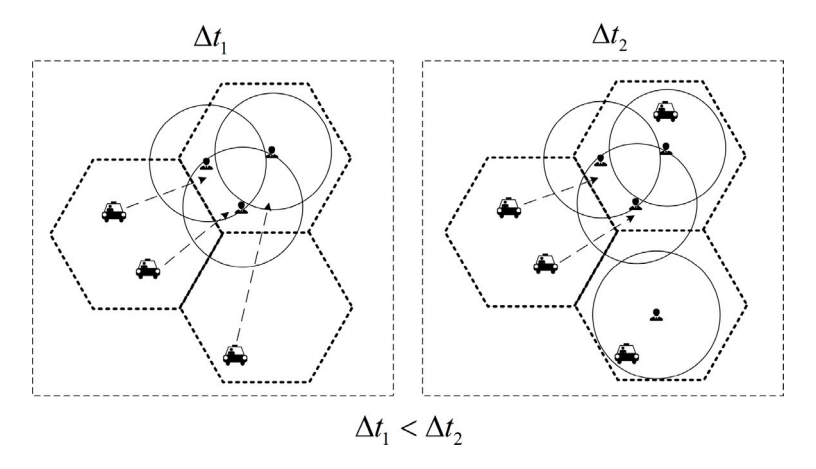


Fig. 2. Joint impact of matching time interval and relocation strategy.

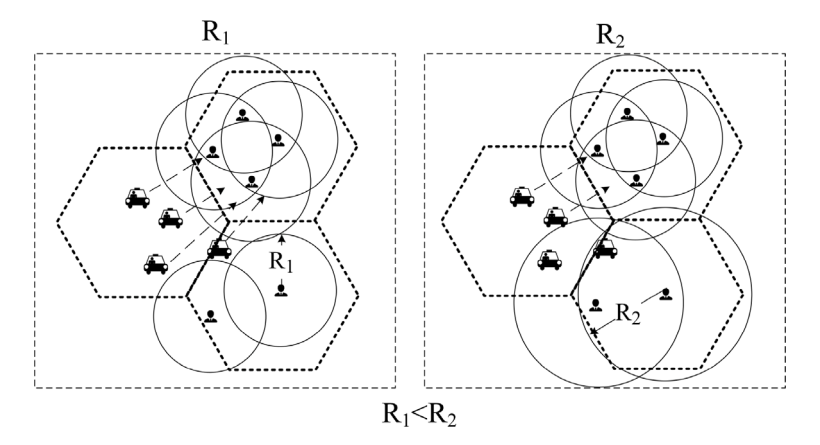


Fig. 3. Joint Impact of matching radius and relocation strategy.

#### 4. Simulation of ride-sourcing systems interacting with traffic congestion

This section elaborates on the details of the proposed simulation model, consisting of two layers: the top layer of the ride-sourcing system (Section 4.2) and the bottom layer of traffic flow (Section 4.1). Specifically, we first propose a multi-region MFD traffic dynamics model and integrate it into a simulation model with hybrid-driven mechanisms (including time-driven and event-driven), which we encapsulate as a module. Further, the ride-sourcing system simulation module implements information exchange by connecting the interface events of the traffic flow simulation module. These two simulation modules communicate with each other. Compared with traffic simulation software like SUMO, our simulation model offers a significant advantage in computational efficiency while maintaining a high level of accuracy in capturing macroscopic congestion features. This characteristic serves as a crucial foundation for enabling simulation-based optimization.

#### 4.1. Traffic flow simulation

In this subsection, first, the notation used in the traffic flow simulation model is given. Next, we introduce the proposed multi-region macroscopic fundamental diagram (MFD) traffic dynamics model. Finally, we provide a detailed description of the implementation of the simulation module based on the proposed traffic dynamics model.

Beojone and Geroliminis (2021) proposed a trip-based MFD traffic dynamics model, which characterizes the entire road network with an MFD and employs the event-driven simulation mechanism. We extended this model from a single region to include multiple sub-regions and utilized a cell transmission model to characterize congestion propagation at region boundaries. Furthermore, a hybrid of time-driven and event-driven mechanisms is proposed to accelerate the simulation process.

#### 4 1 1 Notations

The notations of the traffic flow simulation model are summarized as follows.

```
Indices and sets
```

```
index of sub-region
i
        index of vehicle
j
        index of link
h
        index of node
        the current time of the simulation clock
τ
Z
        set of sub-regions
               set of passengers matched with the vehicle i
\mathcal{M}_{i}\left( 	au\right)
\mathcal{T}_{j}(\tau)
             set of all transfer nodes in the shortest path between the origin and destination of the vehicle j
\mathcal{N}_{i}
          set of all nodes in the sub-region i
         set of links in the sub-region i
\mathcal{D}_{i}^{(\mathrm{R})}(\tau)
               set of the remaining travel distance of all vehicles in the sub-region i, i.e., \forall \{j, d_i^{(R)}(\tau)\} \in \mathcal{D}_i^{(R)}(\tau)
S_i(\tau)
             set of cell transmission model supplies and traffic density for adjacent regional links, i.e., \forall \{s_h(\tau), k_h(\tau)\} \in S_i(\tau)
Q_i(\tau)
             set of cell transmission model demands in sub-region i, i.e. q_b(\tau) \in \mathcal{Q}_i(\tau), q_b represents a queue that follows the
```

 $\mathcal{N}_{i}^{(\text{out})}(\tau)$  set of flows exiting sub-region *i* and entering adjacent sub-regions.

#### **Parameters**

First-In-First-Out (FIFO) principle.

```
free flow speed of a sub-region MFD
v_{\rm f}
        time step of time-driven simulation
Λt
n(\tau)
          the cumulative number of vehicles in the sub-region at time \tau
         the sum of the length of links for all lanes in the sub-region
\Sigma I
\theta, \delta
          parameters of speed-MFD function
\sum_{i^+ \in Z} n_{i^+ i}
                  total flow transferred from adjacent sub-regions
\sum_{i^+ \in Z} n_{ii^+}
                  total flow transferred to adjacent sub-regions
         arrival flow to the destination or exit flow to the system
n^{(d)}
         departure flow within the sub-region
f_b
        flow that transmitted to the link b
        flow that attempts to enter the link b
d_b
        capacity of link b to receive flow
S_b
        traffic density of the link b
k_b
Q^*
         peak value in the flux-MFD
        corresponding critical density of the peak value in the flux-MFD
k^*
p_i^{(MFD)}
             MFD parameters, i.e., p_i^{(\text{MFD})} = \left\{ v_f, \sum l, \delta, \theta, k^*, Q^* \right\}
            current position of the vehicle j
o_j(\tau)
f_{j}(\tau)
            current destination of the vehicle j
            binary variable indicating whether the vehicle j is idle
I_{i}(\tau)
n_i^{(in)}(\tau)
             input flow of sub-region i from other sub-region
```

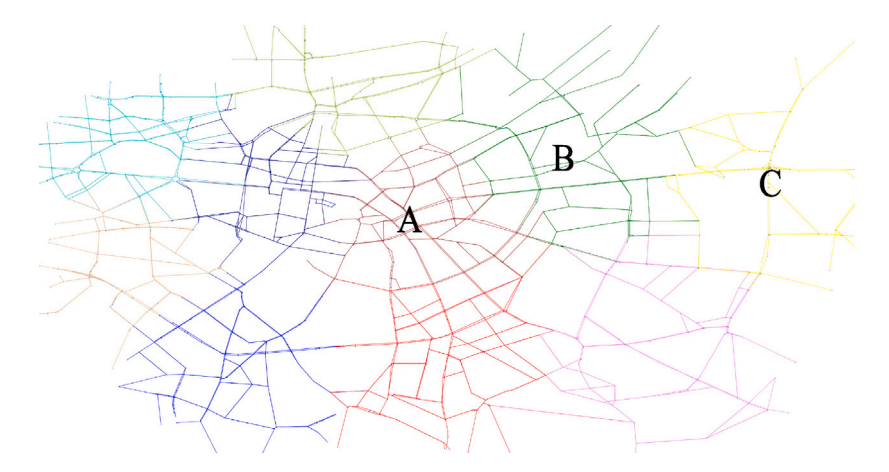


Fig. 4. Regional division of road network.

- $n_i^{(e)}(\tau)$  accumulative number of vehicles in the sub-region *i*
- $n_i^{(d)}(\tau)$  flow departing from the sub-region i
- $n_i^{(a)}(\tau)$  flow exiting the system from the sub-region i
- $\lambda_i(\tau)$  cumulative number of vehicles change rate of the sub-region *i*
- $v_i(\tau)$  instantaneous speed of vehicles in the sub-region i

#### 4.1.2. Traffic dynamics

In the proposed simulation, the road network should be first partitioned into multiple appropriately sized sub-regions to ensure that each sub-region conforms to a reasonable MFD (Geroliminis and Daganzo, 2008). For example, the actual road network with 4062 links in Berlin is divided into 10 sub-regions, as shown in Fig. 4.

In this study, we propose a traffic dynamics modeling approach that distinguishes it from traditional microscopic traffic simulation models. Our approach involves capturing the speed-density relationship of a sub-region by using the speed-MFD (Arnott, 2013), which is derived by fitting a logistic function (see Eq. (1)) to the original MFD data obtained from a microscopic traffic simulation. To access the contribution of each road to the carrying capacity of the road network, we follow the work of Geroliminis and Daganzo (2008) and weigh the raw data accordingly based on the road length and the number of lanes.

$$v(n(\tau)/\Sigma l) = \frac{v_{\rm f} \cdot \delta \cdot e^{-\theta \cdot [n(\tau)/\Sigma l]}}{v_{\rm f} + \delta \cdot \left[e^{-\theta \cdot [n(\tau)/\Sigma l]} - 1\right]} \tag{1}$$

where  $n(\tau)$  represents the cumulative number of vehicles in the sub-region.  $v_{\rm f}$  represents the free flow speed of a sub-region.  $\Sigma l$  represents the total length of all links across all lanes in the sub-region.  $\theta$  and  $\delta$  are adjustment parameters.

Fig. 4 illustrates three examples of road network sub-regions (denoted as A, B, and C) that extend outward from the central city, while Fig. 5 displays the fitted curves of the corresponding speed-MFD and flux-MFD functions. Our analysis indicates that sub-region A reports the highest network density corresponding to the maximum carrying capacity, followed by sub-regions B and C. These findings are consistent with a previous study by Wong et al. (2021). They demonstrated a decline in the free flow speed of the network as the average number of nodes per unit distance increased. This reflects the frequency of network-induced stop-and-go vehicle motion. Furthermore, the network optimal density decreased with the degree density normalized by the trafficable area, signifying the intensity of conflicts between traffic flows. The experimental data from our study validates this assertion as well.

This study adopts the widely accepted fluid approximation assumption, which is commonly employed in the literature (e.g., Lamotte and Geroliminis, 2018). By applying the flow conservation law, the number of vehicles in a given sub-region can be described as follows:

$$n(\tau) = n(t_o) + \int_{t_o}^{t_o + \tau} f_{\text{In}}(t) dt - \int_{t_o}^{t_o + \tau} f_{\text{Out}}(t) dt$$
 (2)

where  $n(t_o)$  represents number of vehicles at initial time  $t_o$ .  $f_{\text{In}}(t) dt$  and  $f_{\text{Out}}(t) dt$  represent the input and output traffic flow in the period  $t_o$  to  $t_o + \tau$ , respectively.

Applying the integral mean value theorem, the discrete formulation for the input/output flow within a simulation step  $\Delta t$  can be written as:

$$\int_{t_o}^{t_o + \tau} f_{\text{In}}(t) dt = f_{\text{In}}(t_o) \tau \approx \frac{\sum_{i \in \mathcal{Z}} n_{i+i} + n^{(b)}}{\Delta t} \tau \tag{3}$$

$$\int_{t}^{t_o + \tau} f_{\text{Out}}(t) dt = f_{\text{Out}}(t_o) \tau \approx \frac{\sum_{i \in \mathcal{Z}} n_{ii^+} + n^{(a)}}{\Delta t} \tau$$
(4)

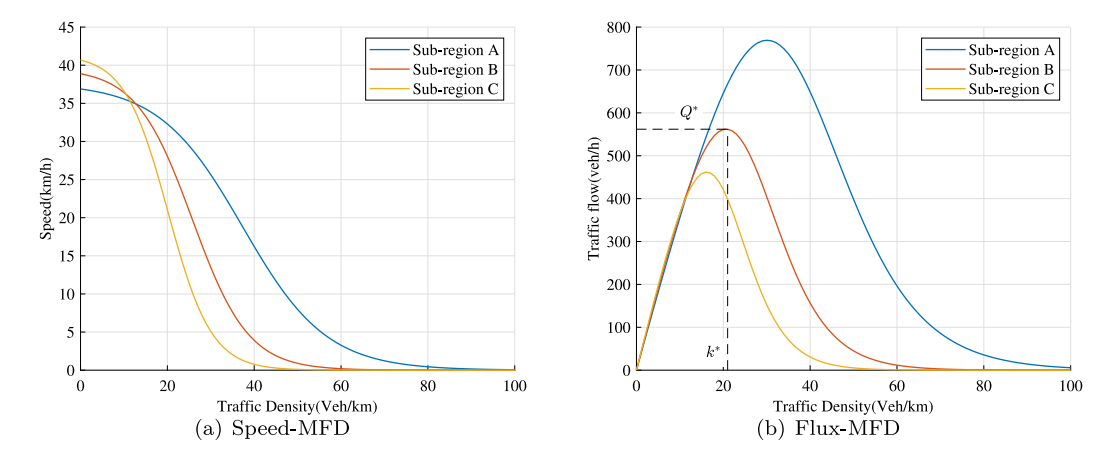


Fig. 5. The MFD for sample sub-regions.

where  $\Delta t$  represents the time step of the time-driven simulation.  $\sum_{i \in \mathbb{Z}} n_{i+i}$  and  $\sum_{i \in \mathbb{Z}} n_{i+i}$  represent total flow transferred from and to adjacent sub-regions  $i^+$ , respectively.  $n^{(a)}$  represents the arrival flow to the destination or exit flow to the traffic system.  $n^{(b)}$  represents departure flow within the sub-region.

Hence, the distance covered by a vehicle during a simulation step  $\Delta t$  can be calculated as:

$$d = \int_{t}^{t_{o} + \Delta t} v(n(\tau) / \Sigma l) d\tau \tag{5}$$

Unlike traditional MFD models that consider the average trip length or trip length distribution of vehicles (e.g., Chen et al., 2022), the approach proposed in this paper updates the remaining trip of vehicles based on the state-dependent speed and shortest path.

Under the assumption of uniform congestion in each sub-region, excessive congestion can result in a stall (Aghamohammadi and Laval, 2019). Therefore, it is necessary to consider the impact of the kinematic wave on the input flow at the boundary between sub-regions. Since the kinematic wave model is a hyperbolic conservation system, the maximum flow across the sub-region boundary can be determined by solving the entropy solution of the corresponding Riemann problem. Alternatively, this problem can be solved by the CTM (Jin, 2017).

Consider a scenario where a node connects two sub-regions, A and B, and all vehicles attempt to enter downstream link b of sub-region B from link a of sub-region A. The flow transmitted to link b can be expressed as:

$$f_b = \min\left\{d_{a,b}, s(k_b)\right\} \tag{6}$$

Here,  $d_{a,b}$  and  $s(k_b)$  refer to the demand and supply in the CTM, respectively. In our simulation model, the demand is updated based on the position and destination of vehicles. As noted by Aghamohammadi and Laval (2019), the supply can be expressed as:

$$s(k_b) = \begin{cases} Q(k_b), k_b \ge k^* \\ Q^*, k_b < k^* \end{cases}$$
 (7)

The critical density and capacity of the flux-MFD are denoted by  $k^*$  and  $Q^*$ , respectively, as shown in Fig. 5(b).

When multiple upstream links of sub-region A transmit vehicles to the link of sub-region B through a boundary node, the flow transmitted can be expanded as follows:

$$f_b = \min\left\{\sum_{a \in A} d_{a,b}, s(k_b) \cdot \mathbb{FI}(a \in A)\right\}$$
(8)

The total demand flow from the upstream links to the downstream link b is given by  $\sum_{a \in A} d_{a,b}$ ,  $s(k_b) \cdot \mathbb{FI}(a \in A)$  denotes the downstream links that supply flow to the upstream links based on the First-In-First-Out (FIFO) principle and the Incremental Transmission (IT) principle. The flow through the regional boundary node depends on both upstream demand and downstream supply, resulting in different exit speeds for each output queue of the regional boundary. This approach accounts for the anisotropy of regional boundary congestion, which is not addressed in the traditional MFD dynamics.

#### 4.1.3. Traffic flow simulation module

The simulation process of the proposed traffic dynamics model is described in Fig. 6. Prior to the vehicle departure event, the shortest path between the origin and destination is obtained. Please note that before the simulation begins, the shortest path data is pre-calculated using the Floyd–Warshall algorithm. It should be emphasized that the shortest path is determined based on distance rather than travel time. The transfer node is identified as the node at the sub-region boundary in the shortest path. According to the traffic dynamics model described, the transfer node is used to determine whether the vehicle enters a new sub-region or waits

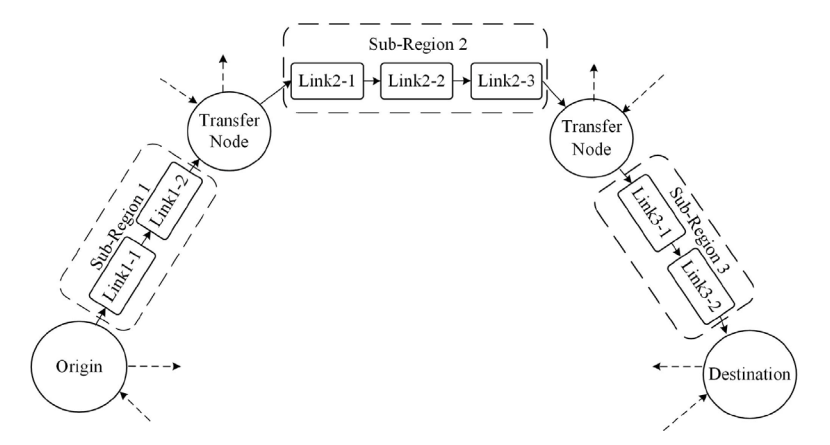


Fig. 6. Traffic flow simulation network.

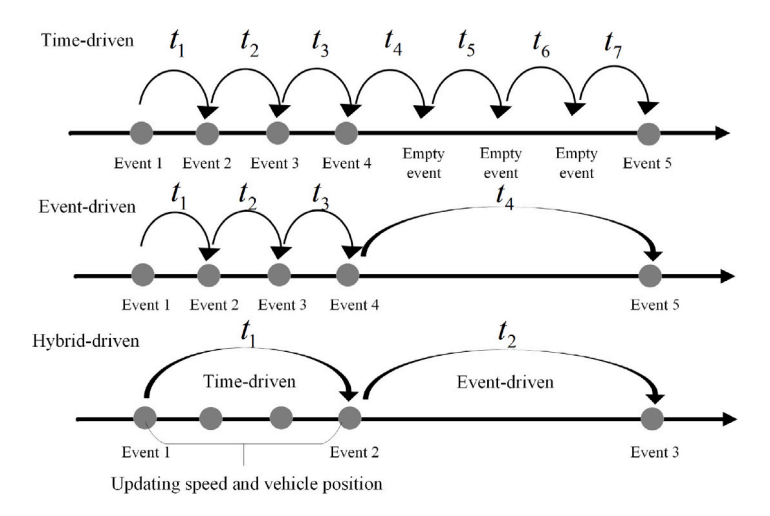


Fig. 7. The difference between three driven mechanisms.

in a queue. Once a vehicle enters a new sub-region, the simulator updates the remaining travel distance and arrival time according to the state-dependent MFD speed.

We adopted the object-oriented discrete event simulation ( $O^2DES$ ) framework developed by Li et al. (2020) to construct our simulation model. The  $O^2DES$  framework describes each module with statics, dynamics, and events.

The time-driven simulation requires a sufficiently small time step to guarantee the simulation's accuracy. Consequently, the event-driven mechanism is commonly considered more efficient than the time-driven for skipping the empty events to further reduce extra update frequency. However, too many events also hamper the simulation computation efficiency. In our model, we assume homogeneous congestion in each sub-region except the boundary, which means that a sub-region updates its congestion status only when vehicles enter or exit it. Enter or exit events occur infrequently. Hence, a longer time step is acceptable in this process. Additionally, a single time-driven event has the capability to update the states of hundreds or even thousands of vehicles in a sub-region, assuming homogeneous congestion. Therefore, our simulation model employs a hybrid-driven mechanism (combining both time-driven and event-driven mechanisms) to advance the simulation process. Specifically, we use this hybrid-driven mechanism in different simulation processes to enhance efficiency and effectiveness. The difference between these three driven mechanisms is shown in Fig. 7.

First, we define the vehicle module. The static attribute only includes a binary parameter  $b_j$ , determining whether the vehicle service is for ride-sourcing passengers. And the dynamic attributes are described as follows:

$$\mathbf{Dynamic.}\ \mathcal{D}_{j}^{(V)} = \left\{o_{j}\left(\tau\right), f_{j}\left(\tau\right), \mathcal{T}_{j}\left(\tau\right), I_{j}\left(\tau\right), \mathcal{M}_{j}\left(\tau\right)\right\}$$

Here,  $o_j(\tau)$  represents the current position of vehicle j at time  $\tau$ .  $f_j(\tau)$  represents destination of the vehicle.  $\mathcal{T}_j(\tau)$  represents the set of all transfer nodes.  $I_j(\tau)$  represents binary variable indicating whether the vehicle is idle.  $\mathcal{M}_j(\tau)$  represents the set of passengers matched with the vehicle.

All events in the vehicle module constitute input events to update the dynamic attributes. Next, we define the traffic flow module for a sub-region, which has the following static attributes:

$$\textbf{Static.} \ \ \mathcal{S}_{i}^{(Z)} = \left\{ \left. \left\{ \left. \mathcal{S}_{b}^{(\mathrm{P})}, \forall b \in \mathcal{P}_{i}. \right. \right\}, \left\{ \left. \mathcal{S}_{n}^{(\mathrm{N})}, \forall n \in \mathcal{N}_{i} \right. \right\}, p_{i}^{(\mathrm{MFD})} \right. \right\}$$

Here,  $S_p^{(P)}, \forall p \in P_i$  refers to the static attributes of links that belong to link set  $P_i$  of sub-region  $i \in \mathcal{Z}$ . These attributes include their lengths, the number of lanes, and the upstream and downstream nodes. Similarly,  $S_n^{(N)}$ ,  $\forall n \in \mathcal{N}_i$  refers to the static attributes of nodes that belong to the node set  $\mathcal{N}_i$  of sub-region i. The attributes include their coordinates, link connections, and the shortest path matrix.  $p_i^{\text{(MFD)}}$  is the MFD parameter set of sub-region i, i.e.,  $p_i^{\text{(MFD)}} = \{v_f, \sum l, \delta, \theta, k^*, Q^*\}$ .

$$\mathbf{Dynamic.} \mathcal{D}_{i}^{(Z)} = \left\{ \begin{array}{l} \mathcal{D}_{i}^{(\mathrm{R})}(\tau), \mathcal{Q}_{i}(\tau), \mathcal{S}_{i}(\tau), n_{i}^{(\mathrm{e})}(\tau), \mathcal{N}_{i}^{(\mathrm{out})}(\tau), \\ n_{i}^{(\mathrm{in})}(\tau), n_{i}^{(\mathrm{d})}(\tau), n_{i}^{(\mathrm{a})}(\tau), \lambda_{i}(\tau), \nu_{i}(\tau) \end{array} \right\}$$

 $\mathbf{Dynamic}. \mathcal{D}_{i}^{(Z)} = \left\{ \begin{array}{l} \mathcal{D}_{i}^{(R)}(\tau), \mathcal{Q}_{i}(\tau), \mathcal{S}_{i}(\tau), n_{i}^{(e)}(\tau), \mathcal{N}_{i}^{(out)}(\tau), \\ n_{i}^{(in)}(\tau), n_{i}^{(d)}(\tau), n_{i}^{(d)}(\tau), n_{i}^{(a)}(\tau), \nu_{i}(\tau) \end{array} \right\}$ Here,  $\mathcal{D}_{i}^{(R)}(\tau)$  represents the set of remaining trip distances of all vehicles in sub-region i at time  $\tau$ .  $\mathcal{Q}_{i}(\tau)$  represents a set of cell transmission model demands in the sub-region.  $S_i(\tau)$  represents a set of cell transmission model supplies and traffic density for adjacent regional links.  $n_i^{(e)}(\tau)$  represents accumulative number of vehicles in the sub-region.  $\mathcal{N}_i^{(\text{out})}(\tau)$  represents a set of flows exiting the sub-region and entering adjacent sub-regions.  $n_i^{(\text{in})}$  represents input flow of sub-region i from other sub-region.  $n_i^{(d)}(\tau)$ represents flow departing from the sub-region.  $n_i^{(a)}(\tau)$  represents flow exiting the system from the sub-region.  $\lambda_i(\tau)$  represents the change rate of the cumulative number of vehicles in the sub-region.  $v_i(\tau)$  represents instantaneous speed of vehicles in the sub-region.

Time-driven, input, internal, and output events are used to drive the simulation process. Time-driven events are triggered with a fixed time step  $\Delta t$ , while all other types of events are triggered conditionally. The event diagram is illustrated in Fig. 8. The detailed relationships are introduced below:

- **Step 1.** Event  $\alpha_i^{(A1)}$  is executed, which triggers the vehicle j to depart from the upper module. The final destination of the vehicle  $f_i(\tau)$  is set, and the shortest path with transit nodes is determined (event  $\alpha_i^{(V2)}$ ). Then, immediately trigger the event  $\alpha_i^{(R1)}$ .
- **Step 2.** The event  $\alpha_{i,j}^{(R1)}$  is executed when vehicle j enters sub-region i. The distance  $d_i^{(R)}(\tau)$  of vehicle j to the first transit node is then obtained. If the vehicle enters from an adjacent sub-region, the density of the adjacent link is updated as  $k_b \leftarrow k_b + 1/l_b$  and the event  $\beta_{i,i}^{(\mathbb{R}^2)}$  is scheduled for time  $\tau + l_b/v(\tau)$ , at which point the vehicle exits the adjacent link and  $k_b$  is updated as  $k_b \leftarrow k_b - 1/l_b$ is performed. If the vehicle reaches the regional boundary or its destination before the next time-driven event update, the exit time  $t_{\text{out}}$  is calculated by Eq. (11). An exit event  $\beta_{i,j}^{(R1)}$  is then triggered at time  $\tau + t_{\text{out}}$ .

  Step 3. Executed event  $\psi_i^{(R1)}$ : Update the cumulative number of vehicles  $n_i^{(e)}(\tau)$  in each sub-region. For all  $i \in \mathcal{Z}$ ,  $n_i^{(e)}(\tau)$  is
- updated as the sum of the number of vehicles driving in the sub-region  $\mathcal{D}_{i}^{(R)}(\tau)$  and the number of vehicles traveling through the sub-region *i* in the queue  $Q_i(\tau)$ , i.e.,  $n_i^{(e)}(\tau) \leftarrow \left| \mathcal{D}_i^{(R)}(\tau) \right| + \sum_{q_b \in Q_i(\tau)} \left| q_b(\tau) \right|$ .
- **Step 4.** Executed event  $\psi_i^{(A1)}$ : Update the link supply  $(\forall s_b \in S_i(\tau))$  of adjacent sub-regions for each sub-region according to
- **Step 5.** The event  $\psi_i^{(R2)}$  is executed, estimating whether vehicles reach the destination or regional boundary before the next time-driven event is triggered, based on their instantaneous speed  $v_i(\tau)$ .  $\forall \left\{j, d_j^{(R)}(\tau)\right\} \in \mathcal{D}_i^{(R)}(\tau)$ : when  $d_j^{(R)}(\tau)/v_i(\tau) < \Delta t$ . If a vehicle attempts to exit the traffic flow from the current sub-region ( $|\mathcal{T}_i(\tau)| = 1$ ), the output flow is updated ( $n_i^{(a)}(\tau) \leftarrow n_i^{(a)}(\tau) + 1$ ). If the vehicle is attempting to cross the sub-region boundary  $\left(\left|\mathcal{T}_{j}(\tau)\right|\neq1\right)$ , the output queue is updated. The vehicles in the queue are allocated to their target links incrementally according to the FIFO principle until the supply is used up. Any remaining vehicles are kept in the queue  $(q_b(\tau) \leftarrow q_b(\tau) \cup \{j\})$ .
- Step 6. Executed event  $\psi^{(A2)}$ : Update the input flow of each sub-region based on the output flow of adjacent sub-regions  $(n_i^{(\text{in})}(\tau) \leftarrow \sum_{i \in \mathcal{Z}} n_i^{(\text{out})}(\tau)).$

**Step 7.** Executed event  $\psi_i^{(R3)}$ : Update the change rate of the accumulative number of vehicles based on Eqs. (3) and (4):

$$\lambda_{i}(\tau) \leftarrow \frac{n_{i}^{(\text{in})}(\tau) + n_{i}^{(\text{d})}(\tau) - \sum n_{i}^{(\text{out})}(\tau) - n_{i}^{(\text{a})}(\tau)}{\Delta t}$$

$$(9)$$

Next, the remaining travel distance of the vehicle is updated, and the vehicle position is also updated by event  $\alpha_i^{(V1)}$ . For each  $\left\{j, d_i^{(R)}(\tau)\right\} \in D_i^{(R)}(\tau)$ , the following update is performed according to Eq. (5):

$$d_j^{(R)} \leftarrow \frac{-v_f}{n_i^{(e)}(\tau) \cdot \theta} \cdot \ln \left[ e^{-\theta \cdot \left( n_i^{(e)}(\tau) + \lambda_i(\tau) \cdot x \right)} + \frac{v_f}{\delta} - 1 \right] \middle| \begin{array}{c} \Delta t \\ 0 \end{array} \right]$$
(10)

If  $d_i^{(R)}(\tau) < 0$ , it indicates that vehicle j has reached the regional boundary or destination within the period  $\Delta t$ . To determine the exact exit time, the bisection method is applied to solve the root of Eq. (11). Subsequently, event  $\beta_{i,j}^{(R1)}$  is triggered at time  $\tau + t_{\text{out}}$ .

$$\frac{-v_{\rm f}}{n_i^{\rm (e)}(\tau) \cdot \theta} \left\{ \ln \left[ \frac{e^{-\theta \cdot (n_i^{\rm (e)}(\tau) + \lambda_i(\tau) \cdot t_{\rm out})} + \frac{v_{\rm f}}{\delta} - 1}{e^{-\theta \cdot n_i^{\rm (e)}(\tau)} + \frac{v_{\rm f}}{\delta} - 1} \right] \right\} = d_j^{\rm (R)}(\tau)$$

$$\tag{11}$$

**Step 8.** Executed event  $\beta_{i,j}^{(R1)}$ : When vehicle j attempts to exit sub-region i, it is removed from the set  $\mathcal{D}_i^{(R)}(\tau)$ . The vehicle's position is updated (event  $\alpha_j^{(V3)}$ ), and its transit nodes are cleared (event  $\alpha_j^{(V3)}$ ). If the vehicle reaches its final destination  $f_j(\tau)$ , the output event  $\gamma_{i,j}^{(A1)}$  is executed, and the upper module takes over the vehicle. Otherwise, it is determined whether the vehicle can enter the downstream sub-region. If  $j \notin q_b(\tau)$  (i.e., the vehicle does not need to wait in the output queue  $q_b$ ), it enters the downstream sub-region, and the event  $\gamma_{i,j}^{(A2)} \to \alpha_j^{(A1)}$  is executed.

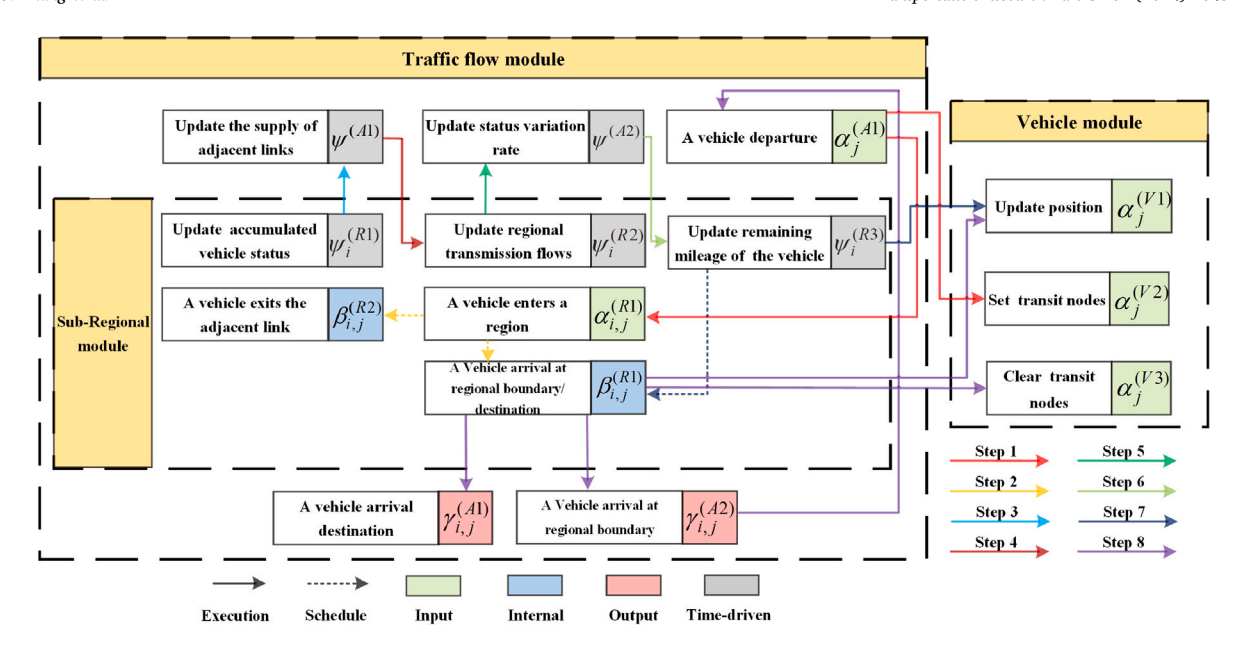


Fig. 8. Triggering relationship and logical flow of the traffic flow module.

#### 4.2. Ride-sourcing system simulation

The ride-sourcing system module is developed based on the traffic flow module. Specifically, a bipartite graph matching strategy, which considers the matching radius, was designed to obtain the passenger-driver pairs. Additionally, a threshold relocation strategy was proposed. This differs from most existing studies that assume drivers always accept relocation tasks, as it allows drivers to refuse them. If a driver accepts a relocation task but fails to reach the predetermined goal, the platform compensates the driver.

#### 4.2.1. Notations

The notations of the ride-sourcing system simulation model are summarized as follows. It is worth noting that an unmatched vehicle, including those nearing the destination of their service mission, idle vehicles, or those relocating, is considered to be an available vehicle.

#### Indices and sets

- c index of passenger request
- C set of all potential passenger requests
- $C_{\mathrm{u},i}(\tau)$  set of unmatched passenger requests in sub-region i
- $C_{\mathbf{u}}(\tau)$  set of all unmatched passenger requests in the matching pool, where  $\forall C_{\mathbf{u},i}(\tau) \in C_{\mathbf{u}}(\tau)$
- $\mathcal{V}_{\mathrm{I},i}\left( au 
  ight)$  set of available vehicles in sub-region i
- $\mathcal{V}_{\mathrm{I}}(\tau)$  set of all available vehicles in the matching pool, where  $\forall \mathcal{V}_{\mathrm{I},i}(\tau) \in \mathcal{V}_{\mathrm{I}}(\tau)$
- $S(\tau)$  set of sub-regions where the number of available vehicles is higher than the upper bound  $S_i^{(u)}$ , where  $\forall s_i(\tau) \in S(\tau)$
- $\mathcal{D}(\tau)$  set of sub-regions where the number of available vehicles is less than the lower bound  $S_i^{(\text{low})}$ , where  $\forall d_i(\tau) \in \mathcal{D}(\tau)$
- $V_{B}(\tau)$  set of background traffic vehicles

## **Parameters**

- $\Delta t_{ij}$  estimated time for vehicle j relocate to sub-region i
- $r_{jc}$  the distance between passenger c and driver j
- $\Delta t_{jc}$  estimated time it takes for vehicle j to pick up passenger c
- $s_i(\tau)$  supply (available vehicles) of relocation strategy in sub-region i
- $d_i(\tau)$  demand (available vehicles) of relocation strategy in sub-region i
- $d_a$  the distance from vehicles to the passengers' destination when the vehicle is included in the matching pool
- $\Delta t_{\rm w}$  maximum wait time of passengers

#### Decision variables

- $x_{jc}$  0–1 variable that determines whether vehicle j matches with passenger c
- $x_{ii}$  decision variable defining the number of vehicles relocated from sub-region i to sub-region i\*
- $R_i$  matching radius in the sub-region i
- $\Delta t_i$  matching time interval for the sub-region i

 $S_i^{(\text{up})}$  upper bound of available vehicles in the sub-region i  $S_i^{(\text{low})}$  lower bound of available vehicles in the sub-region i

#### 4.2.2. Online matching

To describe a typical matching strategy, the following bipartite graph matching model is solved at each time interval  $\Delta t_i$ :

$$\min \sum_{j \in V_{I}(\tau)} \sum_{c \in C_{\mathbf{u},i}(\tau)} \Delta t_{jc} x_{jc} \tag{12}$$

s.t. 
$$\begin{cases} r_{jc} \leq R_{i}, \forall j \in \mathcal{V}_{I}(\tau), \forall c \in \mathcal{C}_{u,i}(\tau) \\ \sum_{c \in \mathcal{C}_{u,i}(\tau)} x_{jc} \leq 1, \forall j \in \mathcal{V}_{I}(\tau) \\ \sum_{j \in \mathcal{V}_{I}(\tau)} x_{jc} \leq 1, \forall c \in \mathcal{C}_{u,i}(\tau) \\ \sum_{j \in \mathcal{V}_{I}(\tau)} \sum_{c \in \mathcal{C}_{u,i}(\tau)} x_{jc} = \min\{|\mathcal{V}_{I}(\tau)|, |\mathcal{C}_{u,i}(\tau)|\} \\ x_{jc} = \{0, 1\}, \forall j \in \mathcal{V}_{I}(\tau), \forall c \in \mathcal{C}_{u,i}(\tau) \end{cases}$$

$$(13)$$

A matching algorithm based on the dominant zone concept proposed by Xu et al. (2017) is designed (Algorithm 1). Each passenger's dominant zone refers to a neighboring area with the passenger as the center. The distance from any point in the area to the passenger is less than the distance between all other passengers and the passenger.

Algorithm 1 is a rule-based heuristic algorithm. Its solutions are superior to those generated by the greedy algorithm following the First-Come, First-Served principle. Furthermore, Algorithm 1 exhibits significantly higher computational efficiency compared to exact algorithms such as the Kuhn–Munkres (KM) algorithm. When considering radius constraints, Algorithm 1 exhibits an algorithm complexity of  $O[|C_{u,i}||\mathcal{V}_1|(|C_{u,i}|+1)]$  in the worst situation. However, the algorithm complexity of the KM algorithm is  $O[|C_{u,i}||\mathcal{V}_1|(|C_{u,i}|+|\mathcal{V}_1|)^3]$  in all situations.

#### Algorithm 1: Matching Algorithm

```
Input: C_{n,i}(\tau); V_{I}(\tau)
    Output: decision variable x_{in}
   foreach c \in C_{n,i}(\tau)\Delta t do
         Set R_c = \emptyset // R_c represents the set of vehicles within radius r_i for the passenger c
 2
 3
         foreach j \in V_I(\tau) do
 4
               if r_{jc} < r_i then
 5
                   R_c \leftarrow R_c \cup \{j\}
 6
 7
         Set R' = \emptyset //R' is set of vehicles within dominant zone of passenger c
 8
 9
               Set i_{\text{domin}} = 1 // Vehicle j in dominant zone of passenger c
10
              foreach c' \in C_{u,i}(\tau) do
11
                    if r_{c'j} < r_{cj} then
12
13
                         i_{\mathsf{domin}} \leftarrow 0
                         break
14
15
                    end
               end
16
               if i_{domin} = 1 then
17
18
                   R'_c \leftarrow R'_c \cup \{j\}
               end
19
20
         end
21
         if |R'| > 0 then
22
               Selecting the vehicle j with the minimum \Delta t_{ic}, x_{ic} = 1
         end
23
24 end
```

#### 4.2.3. Relocation strategy

Improving the matching efficiency can be achieved by dynamically relocating available vehicles from sub-regions with low demand to hot sub-regions. To control the number of idle drivers in each sub-region, we designed a threshold-based relocation strategy.

First, we defined the demand and supply in each region:

$$d_{i}\left(\tau\right) = \begin{cases} S_{i}^{(\text{low})} - \left|\mathcal{V}_{\text{I},i}\left(\tau\right)\right|, \left|\mathcal{V}_{\text{I},i}\left(\tau\right)\right| < S_{i}^{(\text{low})} \\ 0, \left|\mathcal{V}_{\text{I},i}\left(\tau\right)\right| > S_{i}^{\text{low}} \end{cases}$$

$$(14)$$

$$s_{i}(\tau) = \begin{cases} |\mathcal{V}_{I,i}(\tau)| - S_{i}^{(\text{up})}, |\mathcal{V}_{I,i}(\tau)| > S_{i}^{(\text{up})} \\ 0, |\mathcal{V}_{I,i}(\tau)| < S_{i}^{(\text{up})} \end{cases}$$
(15)

$$0 \le S_i^{(\text{low})} < S_i^{(\text{up})} \le \left| \mathcal{V}_{I,i} \left( \tau \right) \right| \tag{16}$$

 $d_i(\tau)$  represents the number of driver shortages in sub-region i. If  $d_i(\tau) > 0$ , the sub-region i is included in the set  $\mathcal{D}(\tau)$ , i.e.  $\forall d_i(\tau) \in \mathcal{D}(\tau)$ ,  $s_i(\tau)$  represents the excess number of drivers in sub-region i. If  $s_i(\tau) > 0$ , the sub-region i is included in the

set  $S(\tau)$ , i.e.  $\forall s_i(\tau) \in S(\tau)$ . Based on the above definition, a typical linear programming model is established, with the objective function of minimizing the time cost of all relocation tasks:

$$\min \sum_{i \in D(\tau)} \sum_{i^* \in S(\tau)} x_{ii^*} \Delta t_{ii^*} \tag{17}$$

$$s.t.\begin{cases} \sum_{i \in D(\tau)} x_{ii^*} \leq s_{i^*}(\tau), \forall i^* \in S(\tau) \\ \sum_{i^* \in S(\tau)} x_{ii^*} \geq d_i(\tau), \forall i \in D(\tau) \\ x_{ii^*} \geq 0 \end{cases}$$

$$(18)$$

The first constraint ensures that the number of relocated drivers in any supply sub-region does not exceed the number of idle drivers in that sub-region. The second constraint represents the supply needed to satisfy all demand sub-regions. The third constraint ensures that all variables are non-negative. Since this is a simple linear programming problem, it can be quickly solved using the commercial solver.

Previous studies generally assumed that drivers would unconditionally obey the relocation instructions of the platform, which does not consistently align with the real-world circumstances. Therefore, we reference a compensation strategy used in the real ride-sourcing platform DiDi Chuxing (Xu et al., 2020a). This strategy displays the relocation instructions on the driver's APP, allowing the acceptance or rejection of these tasks. If a driver is not matched with a passenger within 10 min of arriving at the destination for relocation, the relocation task is considered a failed relocation. Conversely, if a driver is matched with a passenger within 10 min, the relocation task is deemed successful. In order to enhance the execution rate of the dispatch strategy, drivers receive compensation for failed relocations. The amount of compensation is equivalent to the average earnings from one order in the market.

#### 4.2.4. Ride-sourcing system simulation module

This section provides a detailed description of the operating principles of the ride-sourcing simulation module. The static attributes, dynamic attributes, and events embedded in the simulation module are defined as follows, respectively.

Static. 
$$S^{(M)} = \left\{ \left\{ S_i^{(Z)}, \forall i \in \mathcal{Z} \right\}, \left\{ S_c^{(C)}, \forall c \in \mathcal{C} \right\} \right\}$$

Here, the ride-sourcing system module contains all static attributes of the traffic flow module  $(S_i^{(Z)}, \forall i \in \mathcal{Z})$  and passenger requests information (including the departure time, location, and destination)  $S_c^{(C)}, \forall c \in \mathcal{C}$  where  $\mathcal{C}$  is the set of all potential passenger requests.

**Dynamic.** 
$$D^{(M)} = \left\{ \mathcal{V}_{B}(\tau), \mathcal{V}_{I}(\tau), \mathcal{C}_{u}(\tau), S_{i}(\tau), D_{i}(\tau) \right\}$$

Here,  $V_B(\tau)$  represents set of vehicles in the background traffic.  $V_I(\tau)$  and  $C_u(\tau)$  represent set of all available vehicles and unmatched passenger requests in the matching pool, respectively.

As shown in Fig. 9, the ride-sourcing module simulates two processes: the background traffic on the road network and the ride-sourcing service process. In the former process, vehicles depart and complete their trips according to a predefined schedule. The detailed relationships of the ride-sourcing service are as follows.

Step 1. Execute event  $\alpha_j^{(M3)}$ : Initialize the location  $o_j$  of available vehicle j, vehicle j joins the set  $V_1$ , vehicle start cruising (trigger event  $\beta_{c,j}^{(M9)}$ ); then execute event  $\alpha_c^{(M2)}$ :  $\forall c \in C$ , scheduled the event  $\beta_c^{(M4)}$  (passenger c call for service).

Step 2. Execute event  $\beta_c^{(M4)}$ : After a passenger calls for a ride, the passenger is included in the matching pool  $(C_u(\tau) \leftarrow C_u(\tau) \cup \{c\})$ . Event  $\beta_c^{(M5)}$  is scheduled for time  $\tau + \Delta t_w$ , indicating that the order will be canceled because of impatience if  $c \in C_u(\tau)$ , then  $C_u(\tau) \leftarrow C_u(\tau) \setminus \{c\}$ .

Step 3. At intervals of  $\Delta t_i^{\mathrm{m}}$ , executing event  $\psi^{(\mathrm{M1})}$  to match idle drivers with passengers using the bipartite graph matching model described in Section 4.2.2. If  $x_{cj} = 1$ , driver j matches with passenger c, i.e.,  $\mathcal{M}_j(\tau) \leftarrow \mathcal{M}_j(\tau) \cup \{c\}$ . Remove them from the matching pool  $(\mathcal{V}_I(\tau) \leftarrow \mathcal{V}_I(\tau) \setminus \{j\}, \ C_u(\tau) \leftarrow C_u(\tau) \setminus \{c\})$ . Update the vehicle matching status  $(\mathcal{M}_j(\tau) \leftarrow \mathcal{M}_j(\tau) \cup \{c\})$ . The driver starts to pick up the passenger. Vehicle j first temporarily exits the traffic flow module (event  $\alpha_{i,j}^{(\mathrm{R3})}$ ). The vehicle exit from the end node of the link. Then the event  $\gamma_{i,j}^{(\mathrm{M1})} \rightarrow \beta_{c,j}^{(\mathrm{M6})}$  is triggered immediately, and the final destination of the vehicle is set. Finally, the vehicle departs with event  $\alpha_i^{(\mathrm{A1})}$ .

Step 4.  $\gamma_{i,j}^{(\text{A1})} \to \beta_{c,j}^{(\text{M7})}$ , vehicle j arrives at the location of the passenger.  $I_j(\tau) \leftarrow 1$ , i.e., the idle state of the vehicle is updated, then set the vehicle's final destination to the passenger destination. vehicle call to depart (event  $\alpha_j^{(\text{A1})}$ ). When the vehicle approaches the destination  $(d_i^{(\text{R})}(\tau) < d_a, |\mathcal{T}_i(\tau)| = 1)$ , the vehicle is included the matching pool  $(\mathcal{V}_I(\tau) \leftarrow \mathcal{V}_I(\tau) \cup \{j\})$ .

Step 5. When vehicle j arrives at the destination of passenger c, its idle state is updated by setting  $I_j(\tau) \leftarrow 0$ , and it is unmatched with the passenger by removing c from  $\mathcal{M}_j(\tau)$ . If the vehicle is matched with another passenger before reaching its destination (i.e.,  $\left|\mathcal{M}_j(\tau)\right| \neq 0$ ), it departs to pick up the new passenger (event  $\beta_{c,j}^{(\mathrm{M6})}$ ). Otherwise, event  $\beta_j^{(\mathrm{M9})}$  is triggered.

Step 6.  $\beta_j^{(\mathrm{M9})}$  represents that the vehicle starts to cruise. According to model **Assumption 3**, the roulette algorithm determines

**Step 6.**  $\beta_j^{(M9)}$  represents that the vehicle starts to cruise. According to model **Assumption 3**, the roulette algorithm determines whether the driver accepts the relocation task. If the driver accepts the relocation task, a relocation sub-region is designated for the vehicle according to the model solution results described in Section 4.2.3, a destination in that sub-region is randomly selected as the vehicle's final destination, then the vehicle call to depart (event  $\alpha_j^{(A1)}$ ). If the driver does not accept the relocation task, according to model **Assumption 4**, the roulette algorithm is also adopted to determine whether the driver goes to the sub-region with the highest demand, stay, or cruise in the current sub-region.

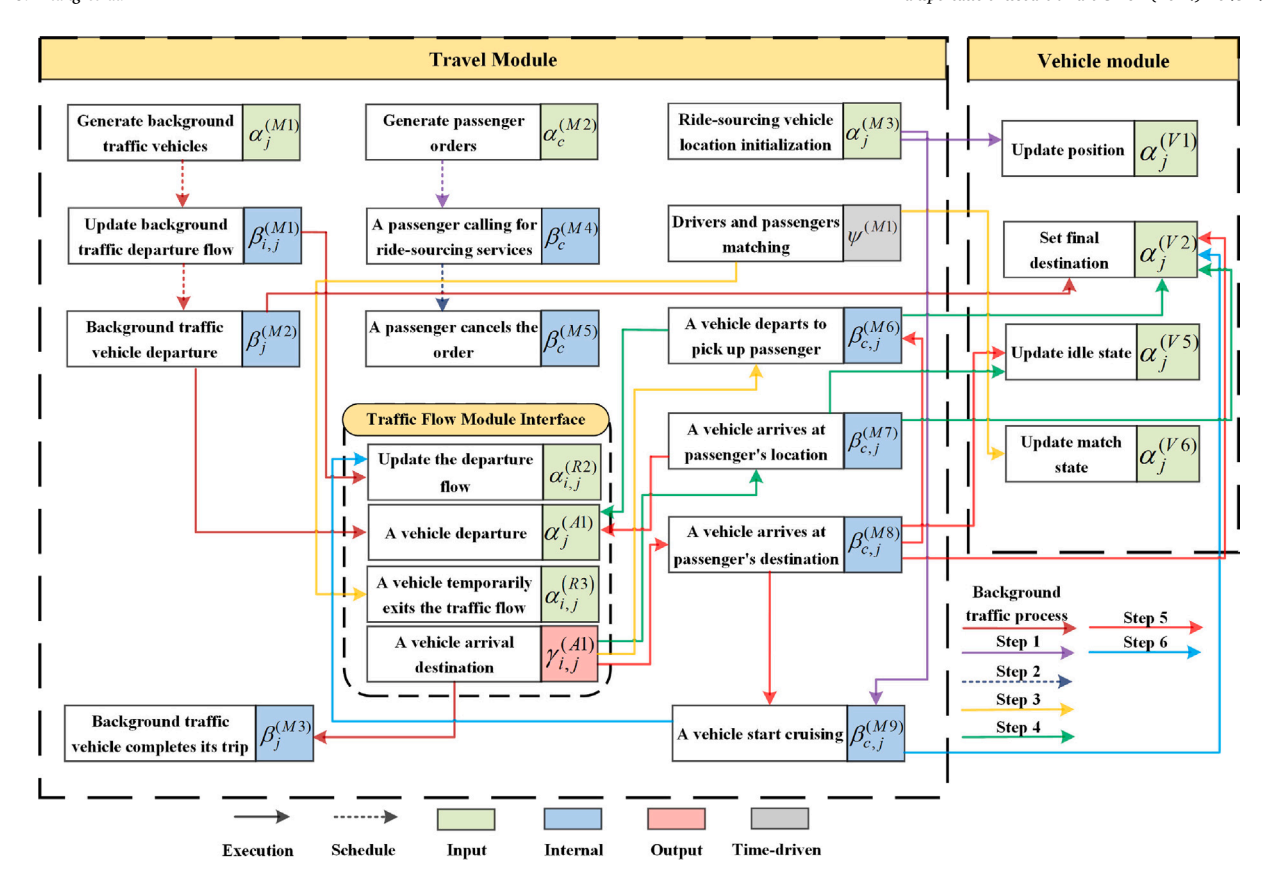


Fig. 9. Triggering relationship and logical flow of the ride-sourcing system module.

#### 5. Simulation-based optimization framework

This section provides a comprehensive overview of the construction of the simulation-based optimization framework. The decision variables in this framework include the matching and relocation strategy parameters. The Bayesian optimization is implemented to solve our problem under a tight computational budget. Some researchers (such as Yang et al. (2023), Dandl et al. (2021)) have used similar approaches to solve complex simulation-based optimization problems. In addition, the rolling horizon approach provides tractability for combining this framework with the prediction model while further improving the efficiency of the Bayesian optimization algorithm in pre-sampling.

First, the optimization model is set with the objective function of maximizing the net income of the platform, which is defined as the difference between the commissions earned on service income and the compensation due to relocation failures.

$$\max f(X) = \eta \cdot \sum_{i \in V} I_j(\rho) - \chi \cdot t_f(\rho)$$
 (19)

$$X = \begin{bmatrix} R_1(\rho) & \Delta t_1(\rho) & S_1^{(\text{up})}(\rho) & \omega_1(\rho) \\ \vdots & \vdots & \vdots & \vdots \\ R_{|\mathcal{Z}|}(\rho) & \Delta t_{|\mathcal{Z}|}(\rho) & S_{|\mathcal{Z}|}^{(\text{up})}(\rho) & \omega_{|\mathcal{Z}|}(\rho) \end{bmatrix}$$

$$(20)$$

$$s.t. \begin{cases} 0 < R_{i}(\rho) < R_{\max}, i = 1, 2, \dots |\mathcal{Z}| \\ 0 < \Delta t_{i}(\rho) < \Delta t_{\max}, i = 1, 2, \dots |\mathcal{Z}| \\ 0 < S_{i}^{(\text{up})}(\rho) < S_{\max}, i = 1, 2, \dots |\mathcal{Z}| \\ \omega_{i}(\rho) = S_{i}^{(\text{low})}/S_{i}^{(\text{up})}, i = 1, 2, \dots |\mathcal{Z}| \\ 0 < \omega_{i}(\rho) < 1, i = 1, 2, \dots |\mathcal{Z}| \end{cases}$$

$$(21)$$

where  $\sum_{j\in V} I_j(\rho)$  represents the total income of all orders within period  $\rho$ .  $\eta$  represents the commission rate for the platform.  $\chi$  represents the compensation cost.  $t_{\Gamma}(\rho)$  represents the number of relocation failures within period  $\rho$ .  $\chi$  is the decision matrix of the joint strategy, which is composed of the matching radius, matching time interval, and the upper bound and lower bound of available drivers of each region in the time period  $\rho$ . As shown in Formula (21), each decision variable specifies its non-negative

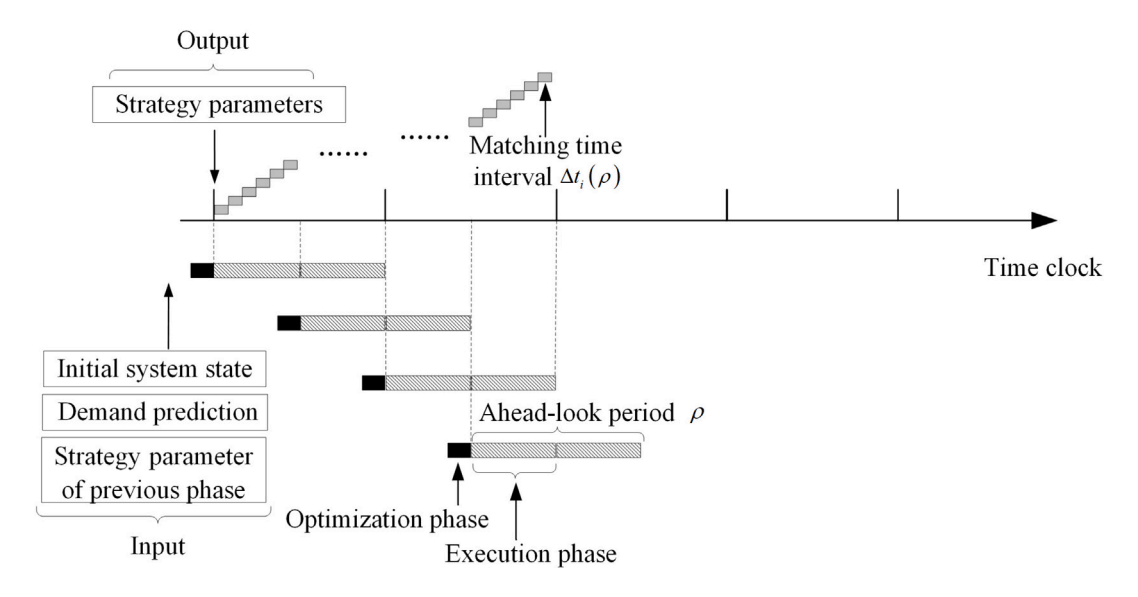


Fig. 10. Rolling horizon approach for simulation-based optimization.

and upper-bound constraints.  $\omega_i(\rho)$  represents the ratio of the lower bound to the upper bound of the available vehicles, ranging from 0 to 1.

Ride-sourcing market operates in a dynamic and stochastic environment, where a rolling horizon approach as shown in Fig. 10 can be adopted to perform the simulation-based optimization framework. Each optimization process includes two phases: the optimization phase and the execution phase. The execution phase represents the latest ahead-look period in simulation-based optimization. The passenger and background traffic demand in the ahead-look periods should be predicted and used as input. Since this paper does not involve a prediction model, so we substitute it with the given demand. The dynamic variation of the driver distribution is deduced by the simulation model, which implies that the input in the simulation-based optimization stage includes the initial state of the system and the prediction of the forward time horizon. In addition, considering the similarity of the demand patterns of the two consecutive periods, the solutions in the previous period are included in the initial sampling of the current optimization phase. In this paper, the operation rolling optimization requires selecting an appropriate number of ahead-look periods to achieve a trade-off between computational efficiency and global optimum. Less ahead-look periods tend to trap in a local optimum. Too many ahead-look periods will trap in a long optimization loop, which is against real-time operational decision-making.

Due to the unavailability of gradient information in this study, the gradient-free algorithm is the only viable option for this simulation-based optimization problem. In this section, a BO framework is employed to solve it. Bayesian optimization is a method used to optimize black-box functions where a black-box function has not an explicit analytic expression. It predicts the output of the function by building a surrogate model. The surrogate model is typically formulated as a Gaussian process model where the next detecting point can be obtained by an acquisition function. During each iteration, Bayesian optimization utilizes known sample points and prior knowledge to update the surrogate model and identifies the location where the current global optimum is most likely to be improved for the subsequent sampling. The improved Gaussian process model and multi-objective acquisition function proposed by Cowen-Rivers et al. (2022) are used in the Bayesian optimization algorithm.

The most common surrogate model in Bayesian optimization is the Gaussian process regression (GP). It is assumed that the objective function to be optimized follows a Gaussian process:

$$f(X) \sim \mathcal{GP}\left(m(X), k_{\theta}\left(X, X'\right)\right)$$
 (22)

where GP is fully specified through a mean function m(X), and a covariance kernel  $k_{\theta}(X, X')$ . The most commonly used GP kernel is stationary, depending only on the norm between x and x', such as the radial basis function kernel:  $k_{\theta}(x, x') = \exp\left(-\frac{\|x - x'\|^2}{2\theta^2}\right)$ .

There have been a number of longitudinal studies reporting that the assumption of stationarity reduces the  $\stackrel{\circ}{GP}$  prediction accuracy, especially when the points collected present a relatively dense distribution in metric measure space (Huo et al., 2023). However, our simulation incorporates numerous random parameters, including the maximum wait time of passengers and the behavior of drivers accepting the relocation task. The assumption of stationarity is not appropriate for our problem.

Snoek et al. (2012) has proved that the input warping transformation assists in handling non-stationary functions. Therefore, we adopt Kumaraswamy input warping transformation as mentioned in Snoek et al. (2012); Kumaraswamy transformation converts the cumulative distribution function (CDF) of the original data to a uniform distribution over the interval [0,1] via the inverse function of the Kumaraswamy distribution. Each input dimension with transformation is given as follows:

$$[\text{Kumaraswamy}_{\gamma}(x_n)]_k = 1 - (1 - [x_n]_k^{a_k})^{b_k} \quad \forall k \in [1:d]$$
 (23)

where  $a_k$  and  $b_k$  are adjustable warping parameters for each of the dimensions, d is the dimension of the problem, and  $\gamma$  represents all parameters, i.e.,  $\gamma = \begin{bmatrix} a_{1:d}, b_{1:d} \end{bmatrix}$ . Thus a GP surrogate with an improved kernel is determined by maximizing the marginal likelihood function:

$$\max_{\theta, \gamma} -\frac{1}{2} Y_n^{\text{T}} (K_{\theta}^{\gamma})^{-1} Y_n - \frac{1}{2} \ln |K_{\theta}^{\gamma}| - \frac{n}{2} \ln (2\pi)$$
 (24)

where  $\theta$  is the parameter in GP kernel, and  $\gamma$  is the parameter for non-stationary transformations.  $Y_n$  is the data observed.  $K_{\theta}^{\gamma}$  represents a covariance matrix that depends on both  $\theta$  and  $\gamma$ , where the new GP kernel  $k_{\theta}^{\gamma}(x,x')=k_{\theta}$  (Kumaraswamy $_{\gamma}(x)$ , Kumaraswamy $_{\gamma}(x')$ ).

When a set of collected data  $\{X,Y\} = \{(x_i,y_i) | i=1,\ldots,n\}$  is known, where X is the input vector and is Y output value. When there is a new input  $X^*$ , to predict the corresponding output  $f(X^*)$ , the joint distribution of  $D = \{X,Y\}$  and set of input points  $X^*$  is given by:

$$\begin{bmatrix} Y \\ f(x^*) \end{bmatrix} \middle| \theta, \gamma \sim \mathcal{N} \left( \begin{bmatrix} m(X) \\ m(X^*) \end{bmatrix}, \begin{bmatrix} \mathbf{K}_{\theta}^{\gamma}(X, X) & \mathbf{K}_{\theta}^{\gamma}(X, X^*) \\ \mathbf{K}_{\theta}^{\gamma}(X^*, X) & \mathbf{K}_{\theta}^{\gamma}(X^*, X^*) \end{bmatrix} \right)$$
(25)

According to the conditional distribution properties of multi-dimensional Gaussian distribution, the posterior predictive  $p(f(X^*)|D) = \mathcal{N}\left(\mu_{\theta,v}(X^*), \sigma_{\theta,v}(X^*)\right)$  with:

$$\mu_{\theta, \gamma}(X^*) = m(X^*) + \mathbf{K}_{\alpha}^{\gamma}(X, X^*)^{\mathsf{T}} \mathbf{K}_{\alpha}^{\gamma}(X, X)^{-1} (Y - m(X))$$
(26)

$$\sigma_{\theta,\gamma}(X^*) = \mathbf{K}_{\rho}^{\gamma}(X^*, X^*) - \mathbf{K}_{\rho}^{\gamma}(X, X^*)^{\mathsf{T}} \mathbf{K}_{\rho}^{\gamma}(X, X)^{-1} \mathbf{K}_{\rho}^{\gamma}(X, X^*)$$

$$(27)$$

Obviously, in a Gaussian process, the prediction result of each point contains not only the predicted value but also the probability distribution of the predicted point. Here, the predicted value is the maximum of  $p(f(X^*)|D)$  when  $f(X^*) = m(X^*) + \mathbf{K}_0^r(X,X^*)^{\mathsf{T}}\mathbf{K}_0^r(X,X^*)^{\mathsf{T}}(Y-m(X))$ .

The acquisition function searches for a better objective function through the prior information from the surrogate model. The acquisition function generates sampling points in the measure space and aims for a better improvement on the objective function. The essence of the acquisition function is a trade-off between exploitation and exploration. Exploitation refers to sampling in measure space where the surrogate model predicts optimal output. Exploration refers to sampling in measure space under conditions of high uncertainty. The goal of both is to maximize the value of the acquisition function to determine the next sampling point. In this study, a multi-objective acquisition function proposed by Cowen-Rivers et al. (2022) is adopted, which considered the following three classical acquisition functions:

#### Upper Confidence Bound (UCB):

$$\alpha_{UCB}(X \mid D) = E\left[\max\left\{\mu_{\theta, Y}(X^*) + \eta \sigma_{\theta, Y}(X^*)\right\}\right] \tag{28}$$

UCB is a simple acquisition function that gives BO the capability of exploration-exploitation trade-off by adjusting parameter  $\eta$ .

# **Expected Improvement (EI):**

$$\alpha_{FI}(X \mid D) = E\left[\max\{f(X^*) - f(X^*)\}\right]$$
(29)

where  $f(X^+)$  represents the most excellent input in the collected data. This means that the purpose of the EI acquisition function is to maximize the expectation of a point larger than the historic optimal point.

# Probability of Improvement (PI):

$$\alpha_{p,f}(X \mid D) = E\left[\max\left\{p\left(f\left(X^{*}\right) - f\left(X^{+}\right) \ge \xi\right)\right\}\right] \tag{30}$$

where  $\xi$  represents a threshold greater than the historic optimal value in the collected data. Therefore, the PI acquisition function maximizes the probability of surpassing the current optimal point with the sampling point.

According to the above three acquisition functions, a multi-objective acquisition seeking a Pareto-front is as follows:

$$\max \left( \alpha_{\text{EI}}(X \mid \mathcal{D}), \alpha_{PI}(X \mid \mathcal{D}), \alpha_{\text{IICB}}(X \mid \mathcal{D}) \right) \tag{31}$$

As the acquisition criteria are changeable, it supports parallel sampling in the solution space. In each iteration, the non-dominated sorting genetic algorithm II (Deb et al., 2002) is employed to select p points from the Pareto front (p=8 in numerical experiments). Subsequently, these selected points are evaluated in parallel through simulation. Additionally, the GPyTorch library is utilized for fitting Gaussian processes, which enables the inference of Gaussian processes with GPU acceleration. This has a pivotal role in the timeliness of strategy optimization in a dynamic simulation environment. The above simulation–optimization procedures are summarized in Algorithm 2.

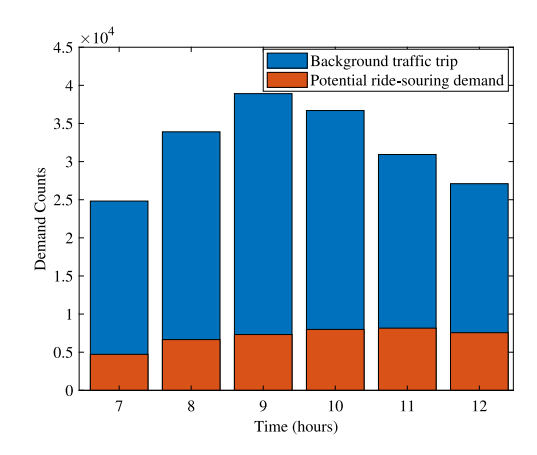


Fig. 11. Distribution of background traffic trips and potential ride-sourcing requests.

#### Algorithm 2: Simulation-optimization procedure

**Input:** Number of initial sampling points  $n_0$ , maximum number of iterations N, kernel function, acquisition function  $\alpha(X|D)$  **Output:**  $X_{\min}$ ,  $Y_{\min}$ 

- 1 Randomly generate a Sobol sequence  $X = \left\{x_0, x_1, \dots, x_{n_0-1}\right\}$ , and evaluate Y via simulation parallelly.
- <sup>2</sup> Estimate parameters ( $\theta$  and  $\gamma$ ) and build posterior probability distribution.
- 3 while n < N do
- 4 Choose the next set of evaluation points  $X^* = \operatorname{argmin} \alpha(X|D)$ .
- 5  $Y^*$  is evaluated parallelly by simulation.
- 6 Update  $X_{\min}$ ,  $Y_{\min}$ .
- 7 Update posterior probability distribution with  $X^*$  and  $Y^*$ .
  - n=n+1
- 9 end

8

#### 6. Computational experiments

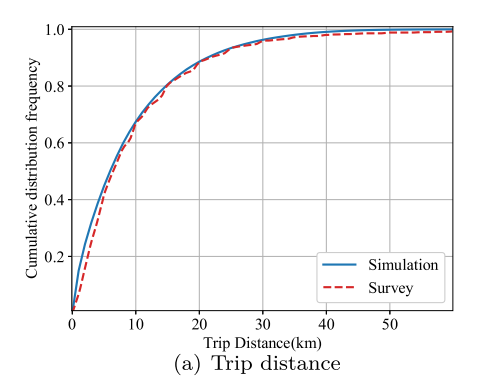
This section presents six groups of computational experiments conducted using the traffic scenario in Berlin. All experiments were executed on a PC equipped with an Intel Core i7-7700 CPU and 8 GB of RAM, operating within a Windows environment. The effectiveness of our proposed method relies on the simulation model and the optimization approach working together. Both components are crucial for addressing our specific problem. Consequently, the initial three groups of experiments focus on testing and analyzing the proposed simulation model. We first verify the efficiency and accuracy of the traffic flow simulation to determine the applicability of simulation-based optimization. Then we investigate the joint impact of the matching radius and time interval in different ride-sourcing fleet size. The third group of experiments explores how fleet size and traffic congestion (including endogenous and exogenous congestion) affect the system performance. This analysis highlights the importance of incorporating endogenous congestion into the operational strategy. The last three groups test and analyze the proposed simulation-based optimization approach. We verify whether the simulation-based optimization framework can make high-quality dynamic joint decisions of matching and relocation strategies within a tight computational budget. Next, we demonstrate the superiority of the proposed dynamic joint optimization strategy compared with two benchmark strategies. Finally, the experiments with different fleet sizes and background traffic demands demonstrate the endogenous congestion (generated by ride-sourcing fleets) should not be ignored. This observation serves as an extension of the findings from the third experiment. Fortunately, these six groups of experiments have vielded unexpected and intriguing findings, allowing us to summarize valuable managerial insights that have exceeded our initial expectations.

#### 6.1. Traffic scenario in Berlin and parameter settings

Our simulation employs the traffic scenario in Berlin Ziemke et al. (2019), which includes automobiles, public transit, walking, and cycling during a typical workday. In Section 6.2, we employed the complete set of scenario data and the entire road network described in Ziemke et al. (2019) to evaluate the accuracy of our simulation. In the remaining subsections, we utilized a portion of the actual road network. This subnetwork was sourced from OpenStreetMap, comprising a total of 4062 links, as illustrated in Fig. 4. The analysis and optimization were conducted within a timeframe of 7:00 to 12:00. Since the scenario data from Ziemke et al. (2019) does not specify whether the agents use taxis or ride-sourcing for travel, a portion of the agents using automobiles were considered as potential ride-sourcing passenger requests, totaling 42,396 requests. The remaining agents were regarded as background traffic

Table 2 Simulation setting.

Simulation setting	Value
Maximum wait time of passenger $\Delta t_{\rm w}$ (min)	$\Delta t_{\rm w} \sim \mathcal{N}(10, 5)$
Probability of drivers cruising to high demand sub-region/staying motionless/cruising within the current sub-region	0.3/0.6/0.1
The probability that the driver accepts the relocation task	0.73
Compensation amount for a failed repositioning task (€)	20
The threshold distance when drivers are included in the matching pool $d_a$ (m)	1000
Time step of continuous simulation $\Delta t$ (s)	15



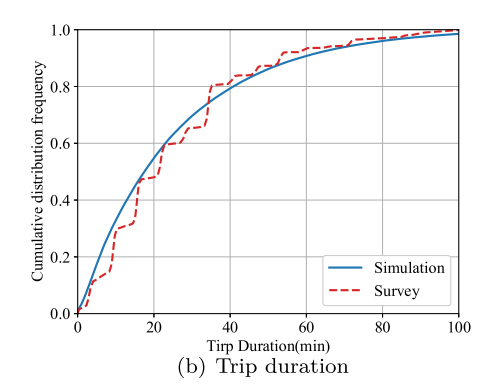


Fig. 12. Simulation accuracy verification.

trips, amounting to a total of 320,619 trips. The distribution of both background traffic trips and potential ride-sourcing requests over time is depicted in Fig. 11. It is important to note that the ride-sourcing demand is likely to be relatively high, which may have an impact on the results in terms of ride-sourcing effects on congestion.

For each order, the fare consists of a fixed fee of  $10 \, \text{\&}$ , a mileage fee of  $2 \, \text{\&}$ per kilometer, and a time fee of  $0.4 \, \text{\&}$ per minute. Since we consider all drivers as registered drivers, the platform does not bear the operating costs but instead takes a 15% commission on each order. Additionally, the unit cost of vehicle fuel consumption for drivers is  $1.8 \, \text{\&}$ per liter.

In this paper, a series of assumptions have been integrated into the simulation model. Now we specify these parameter settings. When a passenger calls for a ride-sourcing service, similar to the approach by Yang et al. (2020), the maximum waiting time of the passenger is established as a random variable following a normal distribution. Regarding drivers, they have the option to reject a relocation task. As elucidated by Xu et al. (2020a), a certain percentage of drivers agree to undertake a relocation task when the platform pledges compensation for unsuccessful relocations. This specified percentage is set as the probability of a driver accepting a relocation task. A certain probability is assigned to their decision of either traveling from a low-demand sub-region to a high-demand sub-region, staying motionless, or cruising within the current sub-region in case a relocation task is rejected (Urata et al., 2021). Notably, when drivers engage in cruising towards a sub-region, the specific destination within that sub-region is selected randomly, irrespective of whether they are cruising independently or in response to a relocation task. For the matching process, drivers are included in the matching pool before completing their ongoing ride. If the current remaining trip distance is below a defined threshold of 1000 m, the driver is included in the matching pool. Additionally, our continuous simulation operates on a time step of 15 s. For clarity, we present a summary of the simulation parameters in Table 2.

#### 6.2. Simulation accuracy and efficiency

Given that the characterization of speed dynamics within a sub-region relies on an aggregated traffic dynamics model, without accounting for congestion variations across individual links. Therefore, it is necessary to verify the accuracy of our traffic simulation model. In pursuit of this, we compared the simulation outcomes with the real-world data from Ziemke et al. (2019). We performed an equivalent simulation utilizing the complete dataset of the entire road network described in Ziemke et al. (2019). It is important to note that we only had access to the real-world cumulative distribution function (CDF) of trip distance and trip duration for verification purposes. Other real data was not accessible to us. As illustrated in Fig. 12, the CDF of trip distances and trip durations in the simulation closely resemble those derived from real-world data. This outcome indicates that the simulated path selection and macroscopic congestion characteristics closely mirror those observed in the real-world scenario.

The computational efficiency of the simulation model is crucial for optimizing operational strategies in the ride-sourcing market, as it is a key factor in determining the applicability of the simulation-based optimization framework. Surprisingly, our simulation model only spends a mean computational time of under 3 s to simulate one hour of the traffic scenario.

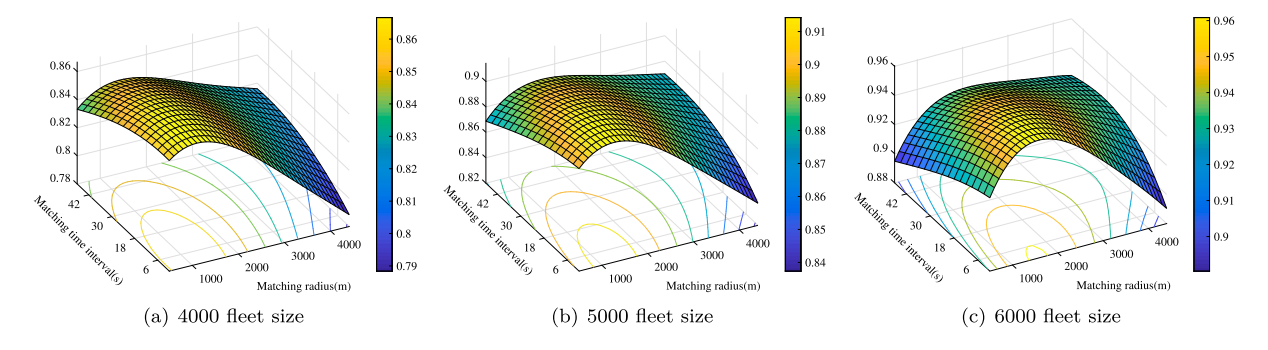


Fig. 13. Joint impact of matching radius and time interval on the matching rate in different fleet sizes.

#### 6.3. Joint impact of matching radius and time interval in different fleet sizes

As elucidated in Section 3, the impact of both the matching radius and the matching time interval extends beyond individual effects, encompassing a joint impact on the system. This joint impact is contingent upon the prevailing supply and demand environment. To investigate this relationship, diverse parameters are input into the simulation model of the ride-sourcing system, enabling observation of the system's response to these variables through the resultant simulation outcomes. In our investigation, the fleet size is set at three different levels: 4000, 5000, and 6000, across various simulation scenarios. Uniform matching radius and matching time interval parameters are applied to all sub-regions within a given simulation. The observation range for the matching radius spans from 500 meters to 4400 m, increasing by 100 meters for each step. Correspondingly, the observation range for the matching interval time ranges from 6 s to 54 s, increasing by 6 s for each step.

Fig. 13 shows the joint effect of the matching radius and time interval on the matching rate in different fleet sizes. As the fleet supply increases, the optimal matching radius increases, and the optimal matching interval time decreases. Evidently, the optimal parameter combination is strongly linked to the existing supply and demand conditions. Consequently, an optimization endeavor must entail a collaborative approach with the relocation strategy to yield the most advantageous outcomes.

These simulation results have similarities and differences with the analytical model's results by Yang et al. (2020). The similarity is that the matching rate is convex with respect to the matching time interval and radius. The difference is that Yang et al. (2020) find that the matching rate is more sensitive to the matching time interval, while our results show that the matching rate is more sensitive to the matching radius (see contour lines in Fig. 13). And Yang et al. (2020) find that the matching rate first increases with the matching radius but then become independent when the matching radius exceeds a certain threshold (about 700 m). But our simulation experiments show that the matching rate first increase and decreases, and it is still affected by the matching radius even at a matching radius of 4400 m. We attribute the reason for these differences to the observation time scale. The study conducted by Yang et al. (2020) focuses on a time scale of a few minutes. During shorter time periods, increasing the matching radius can fulfill more demands until either all demands are met or the supply is depleted. Once the supply is exhausted, expanding the matching radius will no longer have any impact on the system's efficiency. On the other hand, when the observation time scale is larger (such as 1 h in our study), an excessively long pickup distance (matching radius) leads to a loss of efficiency, further worsening subsequent operations.

# 6.4. System performance response to the fleet size and background traffic

The ride-sourcing system's operation performance is affected by traffic congestion. The traffic congestion consists of endogenous congestion (generated by ride-sourcing fleets) and exogenous congestion (generated by background traffic). The objective of this section is to explore the impact of ride-sourcing fleet size and background traffic on the performance of the ride-sourcing system. In this experiment, we have established a total of 119 simulation scenarios with different background traffic scaling factors (spanning from 0.9 to 1.5 times of background traffic trips) and ride-sourcing fleet sizes (ranging from 3500 to 7500 vehicles). The matching radius and matching time interval are uniformly set at 1000 meters and 10 s in all sub-regions, respectively. All drivers in the simulations are engaged in cruising independently.

Most ride-sourcing platforms increase the number of registered drivers to expand their fleet size without restriction to improve the system's performance (the passengers' average waiting time and the total revenue). The limitations of this approach can be seen in Fig. 14.

Interestingly, Fig. 14 shows that the platform's total revenue reaches its peaks with increasing fleet size and then declines, although the platform does not cover vehicle costs. Similarly, passengers' waiting time reaches its minimum and then rises. This is a counter-intuitive observation since it is expected that more ride-sourcing vehicles will generate less passenger waiting time and more platform revenue. After further investigation, it is found that increasing fleet size has two opposing influences on passenger waiting time and platform revenue. That is, increasing the fleet size improves the matching rate and reduces the passenger's waiting time, but it increases road congestion and slows down the circulation of ride-sourcing vehicles, which hurts efficiency. Therefore, limiting

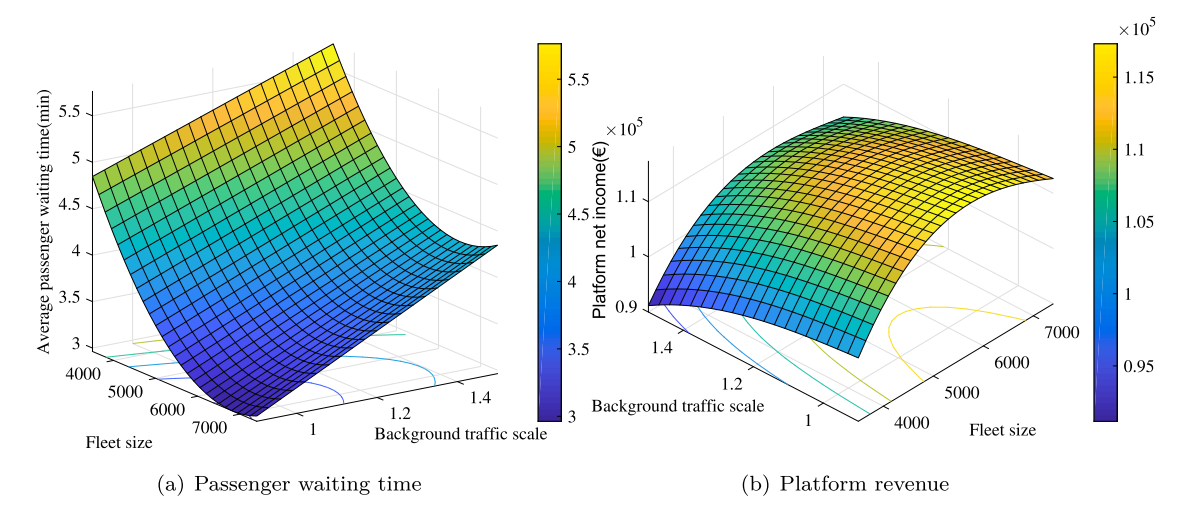


Fig. 14. The impact of fleet size and background traffic congestion on system performance.

Table 3
Calculation time comparison.

Algorithm	Average CPU time per iteration (s)	Total CPU time (s)	
SPSA	9.2 (run three simulations per iteration)	1224	
Traditional BO	5.1 (2.1 s for BO compute)	1725	
Improved BO	6.8 (3.8 s for BO compute)	2150	
Improved BO with parallel sampling	12.1 (4.5 s for BO compute)	439.5	

the fleet size is beneficial to both ride-sourcing platforms and the road transportation system, especially when traffic congestion gets worse.

The insights derived from this analysis are applicable to individual sub-regions, and it is imperative for the platform to consider the adverse consequences stemming from endogenous congestion induced by the fleet. For example, in situations where a sub-region experiences substantial demand, the platform should prudently relocate a large number of drivers to that particular sub-region, especially when the congestion in that sub-region is severe. For the difference between operation strategies with and without consideration of endogenous congestion, we provide a further comparison in Section 6.7.

#### 6.5. Performance of the proposed simulation-based optimization framework

In this section, our objective is to evaluate the performance of the proposed simulation-based optimization framework (Bayesian optimization), comprising convergence and computational time cost. Additionally, we include an evaluation of another gradient-free optimization method called Simultaneous Perturbation Stochastic Approximation (SPSA). SPSA estimates gradient information based on two evaluations of the objective function value. This method has demonstrated successful and widespread application in transportation simulation—optimization problems (Antoniou et al., 2015; Gu and Saberi, 2021).

Fig. 15 shows the comparison of the optimal values of the algorithm iterative process. The optimization period is from 8:00 to 9:00. To ensure a fair comparison, the *x*-axis represents the total number of simulations conducted instead of the iteration round. The discernible trend illustrates that the improved BO algorithm avoids falling into local optimal solutions better than the traditional BO algorithm due to the higher accuracy of the surrogate model fitting and the multi-objective optimization of multiple acquisition functions. Despite its fast initial convergence speed, the SPSA algorithm performs the worst among the four algorithms evaluated. Remarkably, when adopting a parallel sampling strategy, the improved BO algorithm still converges to a good objective function value.

Turning to Table 3, an assessment of the computational CPU times associated with four algorithms is provided. Notably, the improved BO framework entails a relatively higher computational cost compared to both the traditional BO framework and the SPSA. This discrepancy stems from the computation involved in multi-objective acquisition functions. Consequently, the adoption of a parallel sampling strategy becomes imperative to mitigate time overhead, ensuring an acceptable overall time cost for solving.

Finally, we employed the improved BO algorithm with parallel sampling, implementing a rolling optimization approach in a 5000 fleet size scenario over a 1-hour planning horizon. We further compress the computation time of the simulation optimization framework by limiting each phase to 300 simulations, with the initial 90 simulations being randomly sampled. The iterations of the simulation-based optimization framework at each planning horizon are shown in Fig. 16. As each planning horizon of optimization incorporates the decision variables from the previous horizon into the pre-sampling stage except for the first horizon, the initial sampling is not completely random. Especially in horizons 3–6, the objective function value of the first sampling point is

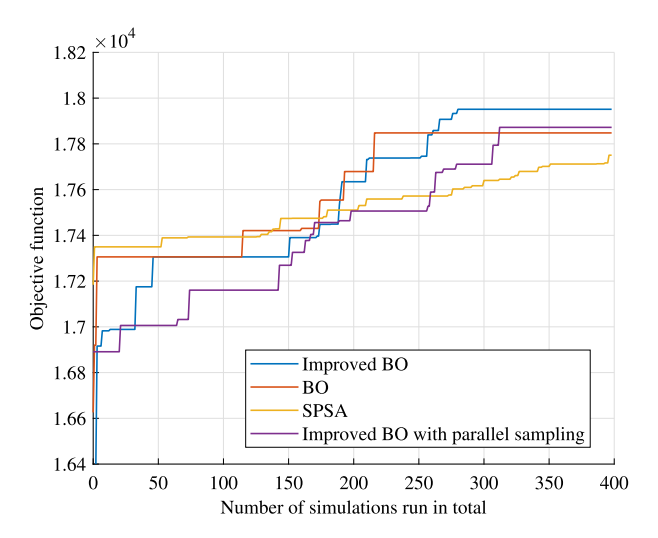


Fig. 15. Algorithm performance comparison.

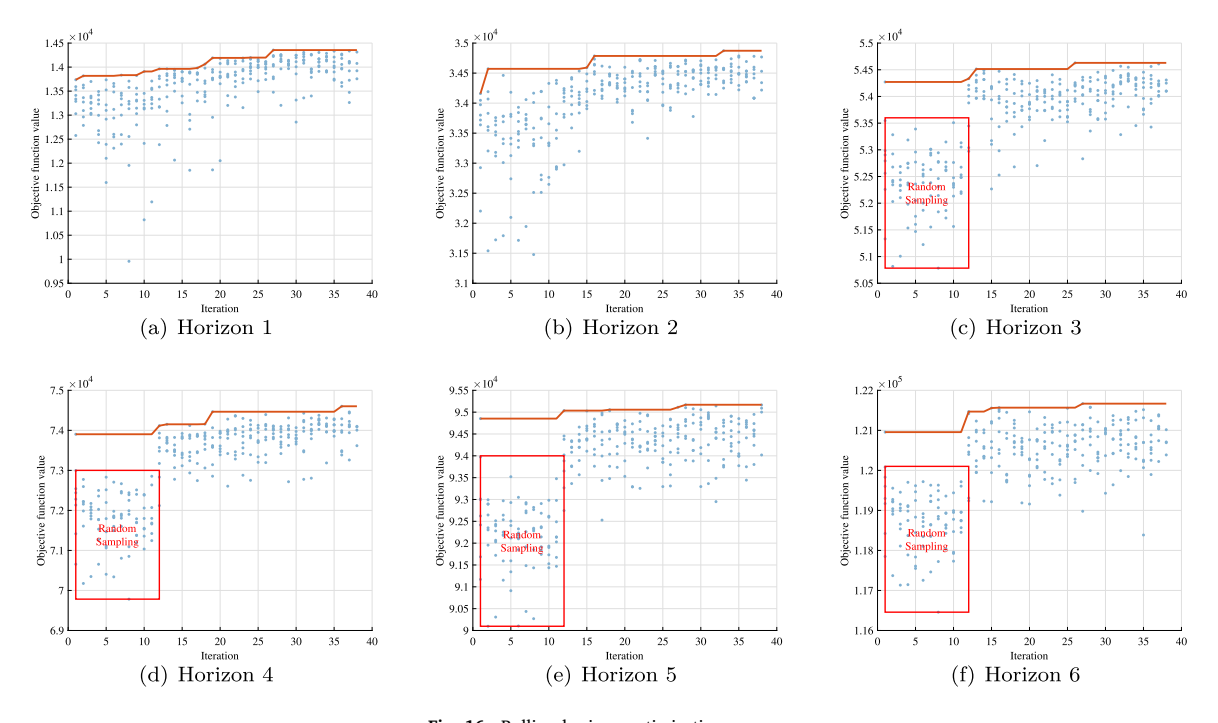


Fig. 16. Rolling horizon optimization process.

significantly superior to the remaining random sampling points. This design improves the efficiency of the pre-sampling, enabling the BO framework to promptly identify a more favorable objective function value region at an earlier stage.

# 6.6. Comparison of dynamic joint optimization and two benchmarks

This section aims to demonstrate the advantages of our proposed dynamic joint optimization strategy. We compare the joint optimization strategy (dynamic matching radius, matching time interval, and vehicle relocation) with two benchmark strategies (fixed matching radius and matching time interval with/without relocation strategies).

As shown in Table 4, our proposed joint optimization strategy is compared with the benchmark strategies. Considering the randomness of the simulation environment, each set of experimental data is the average of the results of 10 simulations, employing the same decision variables yet different random seeds.

First, we tested the optimized relocation strategy with a fixed matching radius and matching time interval. The results from the comparison between the independent cruise (IC) and relocation strategy (RS) in Table 4 demonstrate that accepting the repositioning

Table 4
Optimization result comparison.

MI	MR	PNI		OCR		ADP		DITR		APWT		NART	NRF
		IC	RS	IC	RS	IC	RS	IC	RS	IC	RS	RS	RS
	500	112756	117 058	0.875	0.922	87.43	92.87	0.305	0.267	204	194	3604	200
	1000	115 995	119702	0.899	0.930	91.13	94.63	0.283	0.250	203	191	2092	83
10	2000	115 927	119088	0.896	0.917	91.05	92.73	0.283	0.263	216	212	1448	49
	3000	111 360	114363	0.859	0.873	85.87	86.65	0.308	0.296	238	231	1144	78
	4000	105720	108765	0.813	0.825	79.48	79.77	0.341	0.332	262	253	1203	51
	500	107 911	110544	0.84	0.889	81.96	87.20	0.336	0.300	202	197	3673	256
	1000	112830	118 294	0.877	0.925	87.54	92.74	0.305	0.269	198	193	2076	144
30	2000	114649	119369	0.889	0.918	89.60	92.43	0.291	0.268	206	205	1193	88
	3000	112506	116612	0.871	0.894	87.17	88.99	0.305	0.286	228	220	897	73
	4000	109 233	112797	0.844	0.861	83.46	84.69	0.325	0.308	246	238	963	69
	500	101 165	101 484	0.788	0.833	74.32	78.35	0.372	0.307	225	220	4260	298
	1000	106812	110002	0.831	0.880	80.72	85.99	0.344	0.308	215	208	3018	233
60	2000	109625	113 463	0.853	0.899	83.91	87.87	0.325	0.295	221	213	1802	161
	3000	109 503	112 240	0.851	0.882	83.77	86.61	0.325	0.302	238	233	1479	164
	4000	108 297	110753	0.841	0.869	82.40	84.71	0.333	0.312	252	247	928	154
I	DJO	12	1 667	0.	.945	97	7.14	0.	.246	1	189	925	15

MI: Matching interval (s); MR: Matching radius (m); PNI: Platform net income (€); OCR: Order completion rate; ADP: Average driver profit (€); DITR: Driver idle time rate; APWT: Average passenger waiting time (s); NART: Number of accepted relocation tasks; NRF: Number of relocation failures; IC: Independent cruise; RS: Relocation strategy; DJO: Dynamic joint optimization.

task can improve the system performance level to different degrees, including higher revenue, less passenger waiting time and lower cruising time, compared with the driver's independent cruising.

Furthermore, upon jointly optimizing the repositioning strategy with the matching parameters, the results are noteworthy (see the last row in Table 4). Specifically, the following improvements were observed: the platform net income (PNI) increased by 4.9% to 20.3%, the order completion rate (OCR) advanced by 5.1% to 19.9%, the average driver profit (ADP) increased by 6.6% to 30.7%, the driver idle time rate (DITR) diminished by 3.7% to 12.6%, and the average passenger waiting time (APWT) decreased by 4.5% to 27.9%. It is important to note that the profits of drivers are calculated by deducting the fuel consumption costs of vehicles and adding compensation for failure relocation. Fuel consumption is calculated based on speed and acceleration, following the methodology in Zegeye et al. (2013). These improvements are in comparison to conditions involving driver independent cruising under fixed matching radius and matching time interval settings.

In addition to system efficiency indicators, the failure rate of relocation tasks (NRF/NART) is also one of the important performance measures. This measure assumes added importance as it not only augments the platform's compensation costs but also has a bearing on driver trust in engaging with relocation tasks.

As shown in the last two columns of Table 4, it becomes evident that a reciprocal relationship exists between the matching radius and the number of accepted relocation tasks, as well as the number of task failures. As the matching radius expands, a larger proportion of drivers become actively engaged rather than remaining idle, resulting in a decrease in the pool of available drivers for repositioning tasks. This dynamic interaction between the matching and repositioning strategies underscores their joint influence.

Our findings unequivocally demonstrate that the dynamic joint optimization strategy leads to the lowest count of relocation failures (NRF=15), resulting in the lowest relocation failure rate (NRF/NART=1.62%). Compared to the fixed matching strategy with optimized relocation, the dynamic joint optimization strategy achieved a significant decrease in the relocation failure rate by 1.8% to 15%. This confirms the assertion that integrating the optimized matching strategy enhances the efficiency and effectiveness of the repositioning strategy, leading to superior outcomes.

The advantages of our proposed joint optimization strategy can be further demonstrated by the dynamic variation in the number of passengers and drivers in the matching pool (see Fig. 17). In Fig. 17, the optimal fixed matching strategy refers to the optimal set of fixed parameters (1000 m matching radius and 10 s matching time interval) in the comparison experiment. The use of the optimized repositioning strategy with the optimal fixed matching strategy was able to significantly outperform the independent cruise with the optimal fixed matching strategy.

As described in Section 3, the relocation strategy should be combined with an optimized matching strategy to jointly contribute to system performance. Our experimental results corroborate this idea. The number of passengers in the matching pool was at the lowest level in most of time periods when the joint optimization strategy was activated. The utilization of the fleet under the joint optimization strategy is extremely high because the number of drivers in the matching pool remains low throughout the time period. This indicates that the idle time of drivers is significantly reduced and also indicates that this is not a greedy strategy. A typical greedy strategy, such as using a large matching radius, also keeps the number of drivers in the matching pool consistently low, but the pickup distance increases accordingly. This ultimately reflects an inefficient system performance.

The length of the ahead-look period (horizon length) can impact the effectiveness of our proposed method. Consequently, we evaluated the performance of optimized solutions across various horizon lengths, as shown in Table 5. It is important to note that the optimization time is capped at 8 min. Table 5 illustrates that, while a longer horizon length typically leads to improved global performance, it can also reduce optimization efficiency due to extended simulation times. Therefore, performance measures initially

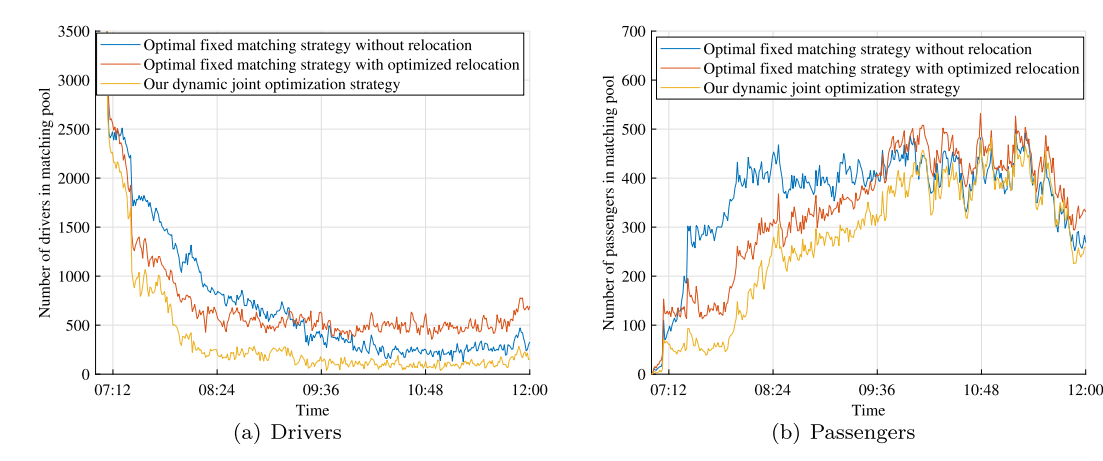


Fig. 17. Dynamics of supply and demand in the matching pool.

Table 5
Comparison of performance measures in different horizon lengths.

Horizon length	Platform net income (€)	Order completion rate	Average driver profit (€)	Average passenger waiting time (s)
1 h	121 677	0.945	97.16	189
1.5 h	122 523	0.949	97.71	188
2 h	121 883	0.948	97.25	189

improve with increasing horizon length but may eventually decline. In summary, given the limited optimization time, the impact of horizon length on optimization performance is somewhat constrained.

#### 6.7. Impact of endogenous congestion on ride-sourcing system decisions

As described in Section 6.4, in urban transportation systems, the ride-sourcing fleets have impacted urban traffic congestion, which feeds back into ride-sourcing operations. Therefore, in this section, we illustrate the importance of integrating the interaction of traffic congestion and ride-sourcing system (i.e., endogenous congestion) into optimizing operational strategies.

We compared the system performance of the optimal solution in scenarios with and without the inclusion of endogenous congestion considerations. This evaluation is carried out across varying background traffic demand scenarios and fleet sizes. Specifically, in the simulation without consideration of endogenous congestion, all vehicles travel at speeds defined by background traffic, i.e., the ride-sourcing fleet does not affect congestion, and other settings remain unchanged. The optimal solution without endogenous congestion effects is then tested in the scenario with endogenous congestion.

In the scenario without endogenous congestion, the main objective of the optimal matching and relocation strategies is to attract as many drivers as possible in high-demand sub-regions. Existing studies have considered the traffic condition but not included the endogenous congestion generated by ride-sourcing fleets, such as Lai et al. (2019). However, in the scenario with endogenous congestion, the optimal matching and relocation strategies should keep a trade-off between satisfying demand and resisting the negative effects of endogenous congestion. This experiment demonstrates the difference.

Figs. 18 and 19 show the gap between the optimal solutions with and without consideration of endogenous congestion. In the two figures, the time delay ratio is calculated as the ratio of the actual time taken to the time it would have taken at free-flow speeds. Considering endogenous congestion not only leads to an increase in system efficiency (Fig. (a) to Fig. (c)), but it also leads to congestion relief (Fig. (d)). This benefit is significantly most pronounced in the scenario with the fleet size of 8000 and a background traffic scaling factor of 1.0, even though relieving traffic congestion was not our initial objective.

As seen in the scenarios with the fleet size of 5000 (background traffic scaling factor 1.0/1.2) and fleet size 8000 (background traffic scaling factor 1.0), this gap gradually increases as the congestion (ride-sourcing fleet size or background traffic) escalates. But in the case of an extreme congestion scenario with fleet size of 8000 and a background traffic scaling factor of 1.2, the time delay ratio reaches around 1.9, and this gap is not as pronounced as the one in the scenario with fleet size of 5,000 and a background traffic scaling factor of 1.2 due to very little space left in the roadway. This result illustrates the advantages of the operational strategy with consideration of endogenous congestion in terms of system performance and shows that our proposed approach enables a win-win situation for both the ride-sourcing system and the road transportation system.

Furthermore, we conducted a geographical analysis to examine the difference between the best solutions with and without consideration of endogenous congestion. For demonstration purposes, we selected the scenario with an 8000 fleet size and a background traffic scaling factor of 1.0. As illustrated in Fig. 20(a), the center sub-region (i.e. sub-region A in Fig. 4) emerges as the primary area impacted by congestion. The congestion also propagates to the surrounding sub-regions, as evidenced by the presence of boundary queues primarily distributed around the center sub-region. In the real world, this center sub-region encompasses portions

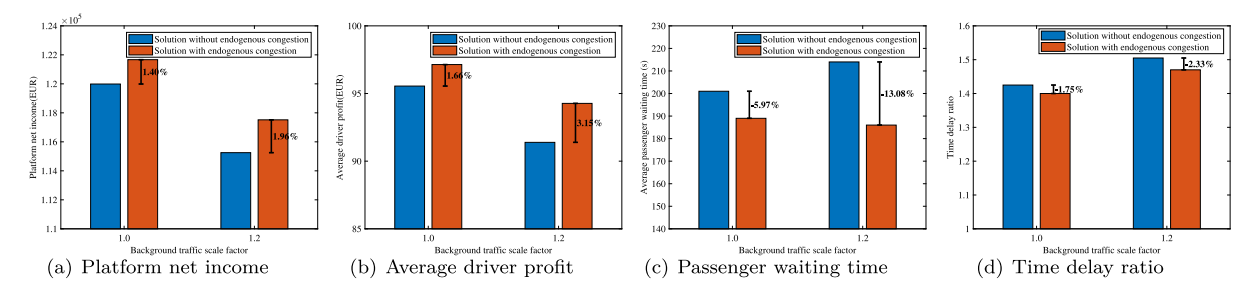


Fig. 18. Comparison of the best solutions with and without endogenous congestion (5000 fleet size).

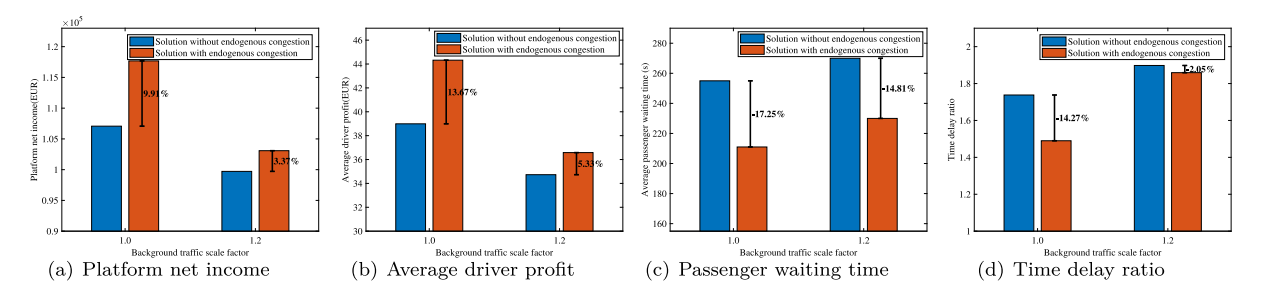


Fig. 19. Comparison of the best solutions with and without endogenous congestion (8000 fleet size).

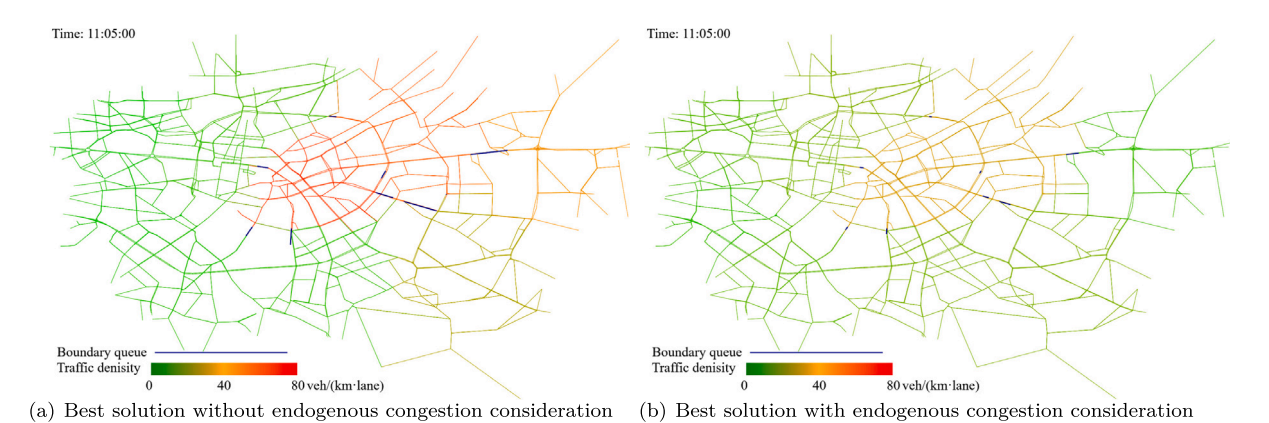


Fig. 20. Geographical analysis for endogenous congestion.

of the Mitte and Friedrichshain-Kreuzberg administrative districts and serves as the political and commercial hub of Berlin. It includes prominent business districts like Alexanderplatz, Friedrichstraße, and Checkpoint Charlie, as well as major thoroughfares such as Hallesches Tor, Potsdamer Platz, and Leipziger Strasse, which experience significant traffic congestion. Therefore, our simulation observations align with the real-world situation. From Fig. 20(a) and (b), the best solution considering endogenous congestion effectively mitigates congestion in the center sub-region. Additionally, the length of the boundary queues is reduced. However, there is still noticeable congestion and boundary queues present when using the best solution without endogenous congestion consideration.

In the simulation model, the determination of shortest paths is based on distance rather than travel time. Therefore, we conducted a comparative analysis of performance measures and simulation times between static routes (based on distance) and dynamic routes (based on congestion). We utilized a scenario involving an 8000-fleet size and a background traffic scaling factor of 1.0. The dynamic routes are generated using the A-star algorithm (Hart et al., 1968). As shown in Table 6, under the best solution without endogenous congestion consideration, dynamic routing resulted in 1.7% higher platform net income compared to static routing. However, the simulation time incurred a 31.0% increase. Under the best solution with endogenous congestion consideration, the system performance remained largely consistent, but there was a 25.8% increase in simulation time.

Table 6
Comparison between static routes and dynamic routes.

Best solution	Routes	PNI	OCR	ADP	APWT	TDR	ST
Without endogenous congestion	Static	107 072	0.806	38.99	255	1.738	4.2
	Dynamic	108 883 (+1.7%)	0.822 (+2.0%)	39.74 (+1.9%)	252 (-1.2%)	1.709 (-1.7%)	5.5 (+31.0%)
With endogenous congestion	Static	117 686	0.916	44.32	211	1.490	3.1
	Dynamic	118 222 (+0.5%)	0.918 (+0.2%)	44.44 (+0.3%)	211	1.487 (-0.2%)	3.9 (+25.8%)

PNI: Platform net income (€); OCR: Order completion rate; ADP: Average driver profit (€); APWT: Average passenger waiting time (s); TDR: Time delay rate; ST: Simulation time (s/h).

#### 7. Conclusion

This work proposes a simulation-based optimization framework to tackle the dynamic joint decision-making problem of matching and relocation strategies in ride-sourcing systems. This problem considers the impact of congestion generated by background traffic and ride-sourcing fleets. The latter reflects the interaction between traffic congestion and the ride-sourcing system operation (i.e., endogenous congestion). The problem can be divided into the online matching problem and the driver relocation problem. The matching radius and time interval for the matching strategy and the upper and lower thresholds for the proposed threshold relocation strategy are jointly and dynamically optimized. Specifically, we first propose a traffic simulation model, which integrates the trip-based and multi-region MFD and CTM, to capture congestion dynamics and propagation among multiple sub-regions. We also design a hybrid of time-driven and event-driven mechanisms to speed up the simulation process. The computational cost of simulating one hour of operation of a ride-souring system is less than 3 s in the traffic scenario of Berlin. Additionally, we ensure the model's accuracy by comparing it with the real data. We integrate the Bayesian optimization, parallel sampling, and rolling horizon approaches to solve this optimization problem. The proposed simulation-based optimization framework can optimize matching and relocation strategy parameters with a planning horizon of 1 h in less than 8 min. Compared with the fixed matching strategy without relocation, our dynamic joint optimization strategy can increase platform net income and driver profit by 4.9%-20.3% and 6.6%-30.7% respectively, and reduce passenger waiting time by 4.5%-27.9%. Moreover, by contrast with the fixed matching strategy with optimized relocation, our dynamic joint optimization strategy significantly reduces the relocation task's failure rate (1.8%-15%). Our simulation and optimization experiments yielded some intriguing findings, with the first two derived from simulation and the last one obtained through optimization:

(1) Yang et al. (2020) show that the matching rate first increases with the matching radius but then becomes independent of the matching radius when the matching radius exceeds a certain threshold (around 700 m). However, our results show that the matching rate first increases and then decreases with the matching radius (a concave function), and it is still affected by the matching radius even at a large matching radius (4400 m). This difference stems from the length of the observation period. The observation time scale of Yang et al. (2020) is small (a few minutes), while our observation time scale is 1 h. This reveals that too long pickup distance (matching radius) downgrades the system's efficiency in the current observation period and further worsens the operation efficiencies in subsequent observation periods. These disadvantages are more and more prominent when the observation period is lengthened. Therefore, there exists a moderate matching radius to maximize the matching rate.

(2) As the fleet size grows, the platform's revenue reaches its peak and then declines, although the platform needs not to cover any vehicle costs. Similarly, passengers' waiting time reaches its minimum and then rises. Interestingly, it demonstrates the trade-off that increasing the fleet size will improve the platform's revenue and reduce the waiting time of passengers but increase road congestion and slow down the circulation of ride-sourcing vehicles, which hurts the system's efficiency and revenue. It also highlights that the platform should consider the negative impact of the endogenous congestion generated by the fleet when relocating vehicles into sub-regions with large demands or heavy congestion.

(3) When the endogenous congestion generated by the ride-sourcing fleet is not considered, the system performance will be estimated optimistically. The resulting optimal operating strategy's performance measures are significantly inferior to those of the optimal operating strategy considering endogenous congestion. That is, considering endogenous congestion not only leads to an increase in the system revenue and efficiency but also leads to congestion relief, even though relieving traffic congestion was not our initial objective. This benefit is the most pronounced when the fleet size and background traffic demand are moderate. This demonstrates that a win-win situation between the ride-sourcing and road transportation systems can be achieved by the optimal ride-sourcing operational strategy with consideration of endogenous congestion.

In future work, our proposed simulation model can be utilized for multi-objective optimization to enhance the ride-sourcing system's efficiency and reduce traffic congestion. Another promising direction would be to investigate the regulation of multiple ride-sourcing platforms to reduce traffic congestion. The existence of numerous ride-sourcing platforms in the same area could lead to a large influx of drivers in an attempt to capture a larger market share, thereby increasing traffic congestion. Therefore, it is crucial to explore regulatory measures to balance market competition and reduce traffic congestion. In addition, combining online optimization with offline optimization is an interesting direction, which has the potential to enhance the solution's quality or expedite the optimization process.

#### CRediT authorship contribution statement

Jun Zhang: Investigation, Methodology, Software, Visualization, Writing – original draft, Conceptualization, Formal analysis. Lu Hu: Conceptualization, Funding acquisition, Investigation, Methodology, Supervision, Writing – review & editing. Yan Li: Methodology. Weiyao Xu: Writing – review & editing. Yangsheng Jiang: Supervision.

#### **Declaration of competing interest**

The authors declare that they have no known competing financial interests or personal relationships that could have appeared to influence the work reported in this paper.

#### Acknowledgments

The work is supported by the National Natural Science Foundation of China (No. 72371209 and 71901183), and the Sichuan Province Department of Science and Technology (No. 24GJHZ0322). The authors are responsible for any remaining errors.

#### References

- Aghamohammadi, R., Laval, J., 2019. A continuum model for cities based on the macroscopic fundamental diagram: a semi-Lagrangian solution method. Transp. Res. Procedia 38, 380–400. http://dx.doi.org/10.1016/j.trpro.2019.05.021, URL: https://linkinghub.elsevier.com/retrieve/pii/\$2352146519300304.
- Alonso-Mora, J., Samaranayake, S., Wallar, A., Frazzoli, E., Rus, D., 2017. On-demand high-capacity ride-sharing via dynamic trip-vehicle assignment. Proc. Natl. Acad. Sci. USA 114 (3), 462–467. http://dx.doi.org/10.1073/pnas.1611675114. URL: https://pnas.org/doi/full/10.1073/pnas.1611675114.
- Antoniou, C., Lima Azevedo, C., Lu, L., Pereira, F., Ben-Akiva, M., 2015. W-SPSA in practice: Approximation of weight matrices and calibration of traffic simulation models. Transp. Res. C 59, 129–146. http://dx.doi.org/10.1016/j.trc.2015.04.030, URL: https://linkinghub.elsevier.com/retrieve/pii/S0968090X15001710.
- Aouad, A., Saritaç, Ö., 2020. Dynamic stochastic matching under limited time. In: Proceedings of the 21st ACM Conference on Economics and Computation. ACM, pp. 789–790. http://dx.doi.org/10.1145/3391403.3399524, Virtual Event Hungary. URL: https://dl.acm.org/doi/10.1145/3391403.3399524.
- Arnott, R., 2013. A bathtub model of downtown traffic congestion. J. Urban Econ. 76, 110–121. http://dx.doi.org/10.1016/j.jue.2013.01.001, URL: https://linkinghub.elsevier.com/retrieve/pii/S0094119013000107.
- Beojone, C.V., Geroliminis, N., 2021. On the inefficiency of ride-sourcing services towards urban congestion. Transp. Res. C 124, 102890. http://dx.doi.org/10.1016/j.trc.2020.102890. URL: https://linkinghub.elsevier.com/retrieve/pii/S0968090X20307907.
- Bertsimas, D., Jaillet, P., Martin, S., 2019. Online vehicle routing: The edge of optimization in large-scale applications. Oper. Res. 67 (1), 143–162. http://dx.doi.org/10.1287/opre.2018.1763, URL: https://pubsonline.informs.org/doi/10.1287/opre.2018.1763.
- Billhardt, H., Fernández, A., Ossowski, S., Palanca, J., Bajo, J., 2019. Taxi dispatching strategies with compensations. Expert Syst. Appl. 122, 173–182. http://dx.doi.org/10.1016/j.eswa.2019.01.001, URL: https://linkinghub.elsevier.com/retrieve/pii/S0957417419300028.
- Bischoff, J., Kaddoura, I., Maciejewski, M., Nagel, K., 2018. Simulation-based optimization of service areas for pooled ride-hailing operators. Procedia Comput. Sci. 130, 816–823. http://dx.doi.org/10.1016/j.procs.2018.04.069, URL: https://linkinghub.elsevier.com/retrieve/pii/S1877050918304290.
- Bischoff, J., Maciejewski, M., 2020. Proactive empty vehicle rebalancing for Demand Responsive Transport services. Procedia Comput. Sci. 170, 739–744. http://dx.doi.org/10.1016/j.procs.2020.03.162, URL: https://linkinghub.elsevier.com/retrieve/pii/S1877050920306220.
- Chen, Z., Wu, W.-X., Huang, H.-J., Shang, H.-Y., 2022. Modeling traffic dynamics in periphery-downtown urban networks combining Vickrey's theory with Macroscopic Fundamental Diagram: user equilibrium, system optimum, and cordon pricing. Transp. Res. B 155, 278–303. http://dx.doi.org/10.1016/j.trb. 2021.12.002, URL: https://linkinghub.elsevier.com/retrieve/pii/S0191261521002277.
- Cowen-Rivers, A.I., Lyu, W., Tutunov, R., Wang, Z., Grosnit, A., Griffiths, R.R., Maraval, A.M., Jianye, H., Wang, J., Peters, J., et al., 2022. Hebo: Pushing the limits of sample-efficient hyper-parameter optimisation. J. Artificial Intelligence Res. 74, 1269–1349.
- Dandl, F., Engelhardt, R., Hyland, M., Tilg, G., Bogenberger, K., Mahmassani, H.S., 2021. Regulating mobility-on-demand services: Tri-level model and Bayesian optimization solution approach. Transp. Res. C 125, 103075. http://dx.doi.org/10.1016/j.trc.2021.103075, URL: https://linkinghub.elsevier.com/retrieve/pii/S0968090X21000991
- Deb, K., Pratap, A., Agarwal, S., Meyarivan, T., 2002. A fast and elitist multiobjective genetic algorithm: NSGA-II. IEEE Trans. Evol. Computat. 6 (2), 182–197. http://dx.doi.org/10.1109/4235.996017, URL: http://ieeexplore.ieee.org/document/996017/.
- Diao, M., Kong, H., Zhao, J., 2021. Impacts of transportation network companies on urban mobility. Nat. Sustain. 4 (6), 494–500. http://dx.doi.org/10.1038/s41893-020-00678-z, URL: http://www.nature.com/articles/s41893-020-00678-z.
- Duan, L., Wei, Y., Zhang, J., Xia, Y., 2020. Centralized and decentralized autonomous dispatching strategy for dynamic autonomous taxi operation in hybrid request mode. Transp. Res. C 111, 397–420. http://dx.doi.org/10.1016/j.trc.2019.12.020, URL: https://linkinghub.elsevier.com/retrieve/pii/S0968090X19306710.
- Erhardt, G.D., Roy, S., Cooper, D., Sana, B., Chen, M., Castiglione, J., 2019. Do transportation network companies decrease or increase congestion? Sci. Adv. 5 (5), eaau2670. http://dx.doi.org/10.1126/sciadv.aau2670, URL: https://www.science.org/doi/10.1126/sciadv.aau2670.
- Feng, S., Ke, J., Xiao, F., Yang, H., 2022. Approximating a ride-sourcing system with block matching. Transp. Res. C 145, 103920. http://dx.doi.org/10.1016/j. trc.2022.103920, URL: https://www.sciencedirect.com/science/article/pii/S0968090X22003333.
- Ge, Y., Xiong, H., Tuzhilin, A., Xiao, K., Gruteser, M., Pazzani, M., 2010. An energy-efficient mobile recommender system. In: Proceedings of the 16th ACM SIGKDD International Conference on Knowledge Discovery and Data Mining KDD '10. ACM Press, Washington, DC, USA, p. 899. http://dx.doi.org/10.1145/1835804.1835918, URL: http://dl.acm.org/citation.cfm?doid=1835804.1835918.
- Geroliminis, N., Daganzo, C.F., 2008. Existence of urban-scale macroscopic fundamental diagrams: Some experimental findings. Transp. Res. B 42 (9), 759–770. http://dx.doi.org/10.1016/j.trb.2008.02.002, URL: https://linkinghub.elsevier.com/retrieve/pii/S0191261508000180.
- Gu, Z., Saberi, M., 2021. Simulation-based optimization of toll pricing in large-scale urban networks using the network fundamental diagram: A cross-comparison of methods. Transp. Res. C 122, 102894. http://dx.doi.org/10.1016/j.trc.2020.102894, URL: https://linkinghub.elsevier.com/retrieve/pii/S0968090X20307944.
- Gueriau, M., Dusparic, I., 2018. SAMoD: Shared autonomous mobility-on-demand using decentralized reinforcement learning. In: 2018 21st International Conference on Intelligent Transportation Systems. ITSC, IEEE, Maui, HI, pp. 1558–1563. http://dx.doi.org/10.1109/TTSC.2018.8569608, URL: https://ieeexplore.jeee.org/document/8569608/.
- Guo, X., Caros, N.S., Zhao, J., 2021. Robust matching-integrated vehicle rebalancing in ride-hailing system with uncertain demand. Transp. Res. B 150, 161–189. http://dx.doi.org/10.1016/j.trb.2021.05.015, URL: https://linkinghub.elsevier.com/retrieve/pii/S0191261521001004.
- Hart, P.E., Nilsson, N.J., Raphael, B., 1968. A formal basis for the heuristic determination. IEEE Trans. Syst. Sci. Cybern.
- Holler, J., Vuorio, R., Qin, Z., Tang, X., Jiao, Y., Jin, T., Singh, S., Wang, C., Ye, J., 2019. Deep reinforcement learning for multi-driver vehicle dispatching and repositioning problem. In: 2019 IEEE International Conference on Data Mining. ICDM, IEEE, pp. 1090–1095.

- Huo, J., Liu, Z., Chen, J., Cheng, Q., Meng, Q., 2023. Bayesian optimization for congestion pricing problems: A general framework and its instability. Transp. Res. B 169, 1–28. http://dx.doi.org/10.1016/j.trb.2023.01.003, URL: https://linkinghub.elsevier.com/retrieve/pii/S0191261523000036.
- Hwang, R.-H., Hsueh, Y.-L., Chen, Y.-T., 2015. An effective taxi recommender system based on a spatio-temporal factor analysis model. Inform. Sci. 314, 28–40. http://dx.doi.org/10.1016/j.ins.2015.03.068. URL: https://dx.doi.org/10.1016/j.ins.2015.03.068. URL: https://dx.doi.org/10.1016/j.ins.2015.03.068.
- Jin, W.-L., 2017. A Riemann solver for a system of hyperbolic conservation laws at a general road junction. Transp. Res. B 98, 21–41. http://dx.doi.org/10. 1016/j.trb.2016.12.007, URL: https://linkinghub.elsevier.com/retrieve/pii/S019126151530196X.
- Ke, J., Xiao, F., Yang, H., Ye, J., 2022. Learning to delay in ride-sourcing systems: A multi-agent deep reinforcement learning framework. IEEE Trans. Knowl. Data Eng. 34 (5), 2280–2292. http://dx.doi.org/10.1109/TKDE.2020.3006084, URL: https://ieeexplore.ieee.org/document/9130935/.
- Ke, J., Yang, H., Zheng, Z., 2020. On ride-pooling and traffic congestion. Transp. Res. B 142, 213–231. http://dx.doi.org/10.1016/j.trb.2020.10.003, URL: https://linkinghub.elsevier.com/retrieve/pii/S0191261520304094.
- Lai, Y., Lv, Z., Li, K.-C., Liao, M., 2019. Urban traffic Coulomb's law: A new approach for taxi route recommendation. IEEE Trans. Intell. Transport. Syst. 20 (8), 3024–3037. http://dx.doi.org/10.1109/TITS.2018.2870990, URL: https://ieeexplore.ieee.org/document/8496857/.
- Lamotte, R., Geroliminis, N., 2018. The morning commute in urban areas with heterogeneous trip lengths. Transp. Res. B 117, 794–810. http://dx.doi.org/10. 1016/j.trb.2017.08.023, URL: https://linkinghub.elsevier.com/retrieve/pii/S0191261517307208.
- Li, H., Cao, X., Sharma, P., Lee, L.H., Chew, E.P., 2020. Framework of O <sup>2</sup> DES.NET digital twins for next generation ports and warehouse solutions. In: 2020 Winter Simulation Conference. WSC, IEEE, Orlando, FL, USA, pp. 3188–3199. http://dx.doi.org/10.1109/WSC48552.2020.9384111, URL: https://ieeexplore.ieee.org/document/9384111/.
- Liu, M., Fang, S., Dong, H., Xu, C., 2021. Review of digital twin about concepts, technologies, and industrial applications. J. Manuf. Syst. 58, 346–361. http://dx.doi.org/10.1016/j.jmsy.2020.06.017, URL: https://linkinghub.elsevier.com/retrieve/pii/S0278612520301072.
- Liu, S., Yue, Y., Krishnan, R., 2015. Non-myopic adaptive route planning in uncertain congestion environments. IEEE Trans. Knowl. Data Eng. 27 (9), 2438–2451. http://dx.doi.org/10.1109/TKDE.2015.2411278, URL: https://ieeexplore.ieee.org/document/7056447/.
- Powell, J.W., Huang, Y., Bastani, F., Ji, M., 2011. Towards reducing taxicab cruising time using spatio-temporal profitability maps. In: Pfoser, D., Tao, Y., Mouratidis, K., Nascimento, M.A., Mokbel, M., Shekhar, S., Huang, Y. (Eds.), In: Advances in Spatial and Temporal Databases, vol. 6849, Springer, Berlin, Heidelberg, pp. 242–260. http://dx.doi.org/10.1007/978-3-642-22922-0\_15, URL: http://link.springer.com/10.1007/978-3-642-22922-0\_15. Series Title. Lecture Notes in Computer Science.
- Qin, G., Luo, Q., Yin, Y., Sun, J., Ye, J., 2021a. Optimizing matching time intervals for ride-hailing services using reinforcement learning. Transp. Res. C 129, 103239. http://dx.doi.org/10.1016/j.trc.2021.103239, URL: https://linkinghub.elsevier.com/retrieve/pii/S0968090X21002527.
- Qin, Z.T., Zhu, H., Ye, J., 2021b. Reinforcement learning for ridesharing: A survey. In: 2021 IEEE International Intelligent Transportation Systems Conference. ITSC, IEEE, Indianapolis, IN, USA, pp. 2447–2454. http://dx.doi.org/10.1109/ITSC48978.2021.9564924, URL: https://ieeexplore.ieee.org/document/9564924/.
- Qin, Z.T., Zhu, H., Ye, J., 2022. Reinforcement learning for ridesharing: An extended survey. Transp. Res. C 144, 103852. http://dx.doi.org/10.1016/j.trc.2022. 103852, URL: https://www.sciencedirect.com/science/article/pii/S0968090X22002716.
- Rong, H., Zhou, X., Yang, C., Shafiq, Z., Liu, A., 2016. The rich and the poor: A Markov decision process approach to optimizing taxi driver revenue efficiency. In: Proceedings of the 25th ACM International on Conference on Information and Knowledge Management. ACM, Indianapolis, Indiana, USA, pp. 2329–2334. http://dx.doi.org/10.1145/2983323.2983689, URL: https://dl.acm.org/doi/10.1145/2983323.2983689.
- Snoek, J., Larochelle, H., Adams, R.P., 2012. Practical Bayesian optimization of machine learning algorithms. arXiv. URL: http://arxiv.org/abs/1206.2944. arXiv:1206.2944 [cs, stat].
- Tang, X., Qin, Z., Zhang, F., Wang, Z., Xu, Z., Ma, Y., Zhu, H., Ye, J., 2019. A deep value-network based approach for multi-driver order dispatching. In: Proceedings of the 25th ACM SIGKDD International Conference on Knowledge Discovery & Data Mining. pp. 1780–1790.
- Urata, J., Xu, Z., Ke, J., Yin, Y., Wu, G., Yang, H., Ye, J., 2021. Learning ride-sourcing drivers' customer-searching behavior: A dynamic discrete choice approach. Transp. Res. C 130, 103293. http://dx.doi.org/10.1016/j.trc.2021.103293, URL: https://linkinghub.elsevier.com/retrieve/pii/S0968090X21003028.
- Vazifeh, M.M., Santi, P., Resta, G., Strogatz, S.H., Ratti, C., 2018. Addressing the minimum fleet problem in on-demand urban mobility. Nature 557 (7706), 534–538. http://dx.doi.org/10.1038/s41586-018-0095-1, URL: http://www.nature.com/articles/s41586-018-0095-1.
- Wang, H., Yang, H., 2019. Ridesourcing systems: A framework and review. Transp. Res. B 129, 122–155. http://dx.doi.org/10.1016/j.trb.2019.07.009, URL: https://linkinghub.elsevier.com/retrieve/pii/S019126151831172X.
- Wong, W., Wong, S.C., Liu, H.X., 2021. Network topological effects on the macroscopic fundamental Diagram. Transportmetr. B: Transp. Dyn. 9 (1), 376–398. http://dx.doi.org/10.1080/21680566.2020.1865850, URL: https://www.tandfonline.com/doi/full/10.1080/21680566.2020.1865850.
- Xu, Z., Li, Z., Guan, Q., Zhang, D., Li, Q., Nan, J., Liu, C., Bian, W., Ye, J., 2018. Large-scale order dispatch in on-demand ride-hailing platforms: A learning and planning approach. In: Proceedings of the 24th ACM SIGKDD International Conference on Knowledge Discovery & Data Mining. ACM, London, United Kingdom, pp. 905–913. http://dx.doi.org/10.1145/3219819.3219824, URL: https://dl.acm.org/doi/10.1145/3219819.3219824.
- Xu, Z., Men, C., Li, P., Jin, B., Li, G., Yang, Y., Liu, C., Wang, B., Qie, X., 2020a. When recommender systems meet fleet management: Practical study in online driver repositioning system. In: Proceedings of the Web Conference 2020. ACM, Taipei, Taiwan, pp. 2220–2229. http://dx.doi.org/10.1145/3366423.3380287, URL: https://dl.acm.org/doi/10.1145/3366423.3380287.
- Xu, Z., Yin, Y., Ye, J., 2020b. On the supply curve of ride-hailing systems. Transp. Res. B 132, 29–43. http://dx.doi.org/10.1016/j.trb.2019.02.011, URL: https://linkinghub.elsevier.com/retrieve/pii/S0191261518311494.
- Xu, Z., Yin, Y., Zha, L., 2017. Optimal parking provision for ride-sourcing services. Transp. Res. B 105, 559–578. http://dx.doi.org/10.1016/j.trb.2017.10.003, URL: https://linkinghub.elsevier.com/retrieve/pii/S0191261517308962.
- Yang, H., Leung, C.W., Wong, S., Bell, M.G., 2010. Equilibria of bilateral taxi-customer searching and meeting on networks. Transp. Res. B 44 (8–9), 1067–1083. http://dx.doi.org/10.1016/j.trb.2009.12.010, URL: https://linkinghub.elsevier.com/retrieve/pii/S0191261509001453.
- Yang, J., Levin, M.W., Hu, L., Li, H., Jiang, Y., 2023. Fleet sizing and charging infrastructure design for electric autonomous mobility-on-demand systems with endogenous congestion and limited link space. Transp. Res. C 152, 104172. http://dx.doi.org/10.1016/j.trc.2023.104172, URL: https://www.sciencedirect.com/science/article/pii/S0968090X23001614.
- Yang, H., Qin, X., Ke, J., Ye, J., 2020. Optimizing matching time interval and matching radius in on-demand ride-sourcing markets. Transp. Res. B 131, 84–105. http://dx.doi.org/10.1016/j.trb.2019.11.005, URL: https://linkinghub.elsevier.com/retrieve/pii/S0191261518311731.
- Yu, X., Gao, S., Hu, X., Park, H., 2019. A Markov decision process approach to vacant taxi routing with e-hailing. Transp. Res. B 121, 114–134. http://dx.doi.org/10.1016/j.trb.2018.12.013, URL: https://linkinghub.elsevier.com/retrieve/pii/S0191261518303837.
- Zegeye, S., De Schutter, B., Hellendoorn, J., Breunesse, E., Hegyi, A., 2013. Integrated macroscopic traffic flow, emission, and fuel consumption model for control purposes. Transp. Res. C 31, 158–171. http://dx.doi.org/10.1016/j.trc.2013.01.002, URL: https://linkinghub.elsevier.com/retrieve/pii/S0968090X13000041.
- Zhao, B., Xu, P., Shi, Y., Tong, Y., Zhou, Z., Zeng, Y., 2019. Preference-aware task assignment in on-demand taxi dispatching: An online stable matching approach. In: AAAI. Vol. 33, pp. 2245–2252. http://dx.doi.org/10.1609/aaai.v33i01.33012245, URL: https://www.aaai.org/ojs/index.php/AAAI/article/view/4060.
- Zhou, X., Rong, H., Yang, C., Zhang, Q., Khezerlou, A.V., Zheng, H., Shafiq, Z., Liu, A.X., 2020. Optimizing taxi driver profit efficiency: A spatial network-based Markov decision process approach. IEEE Trans. Big Data 6 (1), 145–158. http://dx.doi.org/10.1109/TBDATA.2018.2875524, URL: https://ieeexplore.ieee.org/document/8492462/.
- Ziemke, D., Kaddoura, I., Nagel, K., 2019. The MATSim Open Berlin Scenario: A multimodal agent-based transport simulation scenario based on synthetic demand modeling and open data. Procedia Comput. Sci. 151, 870–877. http://dx.doi.org/10.1016/j.procs.2019.04.120, URL: https://linkinghub.elsevier.com/retrieve/pii/S1877050919305848.